AFRL-RZ-WP-TP-2012-0117

ANALYTICAL STUDY: TEMPERATURE VARIATION ACROSS THE HEATED SURFACE OF A POST WITH CONVECTIVE SIDEWALL COOLING (PREPRINT)

Kirk L. Yerkes and Kelli Ashbrook

Energy/Power/Thermal Division

APRIL 2012

AIR FORCE RESEARCH LABORATORY
PROPULSION DIRECTORATE
WRIGHT-PATTERSON AIR FORCE BASE, OH 45433-7251
AIR FORCE MATERIEL COMMAND
UNITED STATES AIR FORCE

REPORT DOCUMENTATION PAGE

Form Approved
OMB No. 0704-0188

1. REPORT DATE *(DD-MM-YY)*	2. REPORT TYPE	3. DATES COVERED *(From - To)*
April 2012	Technical Paper Preprint	01 September 2011 – 01 April 2012

4. TITLE AND SUBTITLE
ANALYTICAL STUDY: TEMPERATURE VARIATION ACROSS THE HEATED SURFACE OF A POST WITH CONVECTIVE SIDEWALL COOLING (PREPRINT)

5a. CONTRACT NUMBER
In-house

5b. GRANT NUMBER

5c. PROGRAM ELEMENT NUMBER
62203F

6. AUTHOR(S)
Kirk L. Yerkes (AFRL/RZPE)
Kelli Ashbrook (APRL/RZPS)

5d. PROJECT NUMBER
3145

5e. TASK NUMBER
13

5f. WORK UNIT NUMBER
31451311

7. PERFORMING ORGANIZATION NAME(S) AND ADDRESS(ES)
Energy and Power Systems Branch (AFRL/RZPE)
Thermal and Electrochemical Branch (AFRL/RZPS)
Energy/Power/Thermal Division
Air Force Research Laboratory, Propulsion Directorate
Wright-Patterson Air Force Base, OH 45433-7251
Air Force Materiel Command, United States Air Force

8. PERFORMING ORGANIZATION REPORT NUMBER
AFRL-RZ-WP-TP-2012-0117

9. SPONSORING/MONITORING AGENCY NAME(S) AND ADDRESS(ES)
Air Force Research Laboratory
Propulsion Directorate
Wright-Patterson Air Force Base, OH 45433-7251
Air Force Materiel Command
United States Air Force

10. SPONSORING/MONITORING AGENCY ACRONYM(S)
AFRL/RZPE

11. SPONSORING/MONITORING AGENCY REPORT NUMBER(S)
AFRL-RZ-WP-TP-2012-0117

12. DISTRIBUTION/AVAILABILITY STATEMENT
Approved for public release; distribution unlimited.

13. SUPPLEMENTARY NOTES
Paper contains color.
PA Case Number: 88ABW-2012-1993; Clearance Date: 04 Apr 2012.

14. ABSTRACT

Often it is desirable to cool electronic components to minimize the temperature gradient across the heat generating surface. This isothermal requirement is often required to in order to minimize thermal stresses, in the case of power electronics, or in the case of laser components, such as laser diodes, to minimize optical distortion.

The objective of this analysis is to determine the effects of boundary condition(s) that will influence the steady-state temperature gradient along the top heated surface of cylindrical and rectangular posts. This is accomplished by casting the dimensionless analytical solutions in graphical form similar to Heisler-Gröber Charts. Both dimensional and dimensionless analytical solutions are presented followed by graphical presentations in dimensionless form.

In this manner, the "best" boundary conditions can be used to specify the cold plate requirements to optimally cool the electronics package. The generated dimensionless plots also allow for easy graphical determination of these boundary conditions as defined in a dimensionless form which can be readily interpreted and used to determine optimal dimensional geometries and/or thermo physical material properties to minimize temperature gradients across a heated electronic surface.

15. SUBJECT TERMS
electronics cooling, heat transfer, convection, conduction

16. SECURITY CLASSIFICATION OF:			17. LIMITATION OF ABSTRACT:	18. NUMBER OF PAGES	19a. NAME OF RESPONSIBLE PERSON (Monitor)
a. REPORT	b. ABSTRACT	c. THIS PAGE			Jim Scofield
Unclassified	Unclassified	Unclassified	SAR	42	19b. TELEPHONE NUMBER *(Include Area Code)* N/A

TABLE OF CONTENTS

LIST OF FIGURES

NOMENCLATURE

A	cross sectional area, m^2
b	half width of the rectangular slab or radius of cylinder, m
Bi	Biot number, hb/k
H	h/k
h	convective heat transfer coefficient $W/(m^2 \cdot K)$
L	height of rectangular slab or cylinder, m
k	thermal conductivity $W/(m \cdot K)$
Q	heater input power, W
r	dimensional coordinate, m
R	dimensionless coordinate, r/b
T	temperature, K
T_∞	temperature of surroundings
y	dimensional coordinate, m
Y	dimensionless coordinate, y/b
Z	dimensional coordinate, m
Z	dimensionless coordinate, z/b

Greek

β_m	eigenvalue
η	dimensionless heat input, $b(Q/A)/(k(T_c-T_\infty))$
θ	dimensionless temperature
ξ	aspect ratio, L/b

1.0 EXECUTIVE SUMMARY

Often it is desirable to cool electronic components to minimize the temperature gradient across the heat generating surface. This isothermal requirement is often required to in order to minimize thermal stresses, in the case of power electronics, or in the case of laser components, such as laser diodes, to minimize optical distortion.

The objective of this analysis is to determine the effects of boundary condition(s) that will influence the steady-state temperature gradient along the top heated surface of cylindrical and rectangular posts. This is accomplished by casting the dimensionless analytical solutions in graphical form similar to Heisler-Gröber Charts. Both dimensional and dimensionless analytical solutions are presented followed by graphical presentations in dimensionless form.

In this manner, the "best" boundary conditions can be used to specify the cold plate requirements to optimally cool the electronics package. The generated dimensionless plots also allow for easy graphical determination of these boundary conditions as defined in a dimensionless form which can be readily interpreted and used to determine optimal dimensional geometries and/or thermo physical material properties to minimize temperature gradients across a heated electronic surface.

2.0 INTRODUCTION

Often it is desirable to cool electronic components in such a manner as to minimize the temperature gradient across the heat generating surface. This isothermal requirement is often required to in order to minimize thermal stresses, in the case of power electronics, or in the case of laser components, such as laser diodes, to minimize optical distortion. Traditionally, electronics cooling has been accomplished by mounting cold plates or cooling fins to the electronics package. In doing so, the "best" cooling approach was typically taken from a thermal management "tool box" consisting of proven concepts. This bolt-on approach to electronics thermal management is only partially effective and does little to optimize the thermal management of electronics with regard to minimizing thermal stresses within the electronics package. Another option to electronics thermal management is to define the boundary conditions in order to minimize thermal stresses within the electronics package generating the heat. The specific cooling approach is then designed to optimally match the boundary conditions that will minimize thermal stresses within the electronics package. Once this is done one can account for the necessary thermal management components needed to transport the heat to the final heat sink. Yovanovich[1] investigated thermal spreading resistances in a finite circular cylinder with side and end cooling. He developed a general dimensionless analytical solution, for a circular heat source, showing that the dimensionless thermal resistance depended upon four dimensionless system parameters; relative heat source size, relative cylinder thickness, and side and end surface Biot numbers. Muzychka[2] followed up on the research of Yovanovich and examined the dimensionless analytical solutions for the thermal spreading resistance of circular cylinder and rectangle geometries. These solutions addressed geometries consisting of both isotropic and compound systems and resulted in simple expressions to determine the impact of edge cooling on the thermal spreading resistance. However, these studies do not take into account temperature variation at the heated surface.

The objective of this analysis is to determine the effects of boundary condition(s) that will influence the steady-state temperature gradient along the top heated surface of cylindrical and rectangular posts. This is accomplished by casting the dimensionless analytical solutions in graphical form similar to Heisler-Gröber Charts.[3-5] Both dimensional and dimensionless analytical solutions are presented followed by graphical presentations in dimensionless form.

3.0 ANALYTICAL FORMULATION

A simplified example of this analytic approach, in rectangular and cylindrical, dimensional and dimensionless forms, is shown in Figure 1. In this example, a uniform and constant heat flux is applied to the top surface of a solid material. The centerline of the material lies along $y = Y = 0$ or $r = R = 0$ and is defined as an adiabatic surface. A convective boundary of the third kind lies along $y,r = b$ *or* $Y,R = 1$ and is bounded by temperature, T_∞. The base of the material represents a cold plate, that is a boundary condition of the first kind, at a fixed constant temperature $T = T_c$ *or* $\theta = 1$.

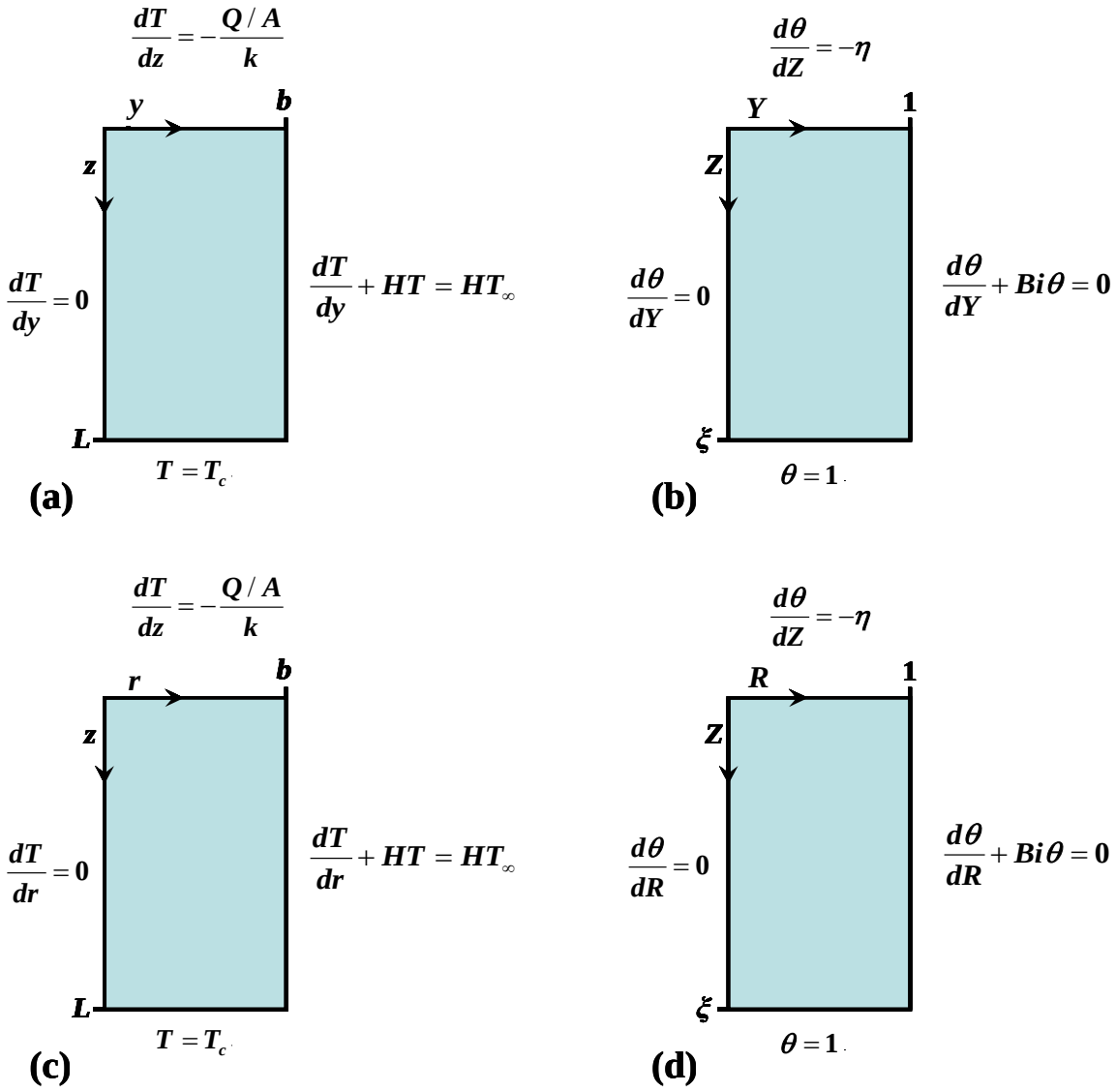

Figure 1. Example for (a) rectangular, dimensional case; (b) rectangular, dimensionless; (c) cylindrical, dimensional case; and (d) cylindrical, dimensionless case.

3.1 Rectangular

The dimensionless form of the example shown in Figure1b is formulated using the dimensionless parameters

$$\theta = \frac{(T - T_\infty)}{(T_c - T_\infty)},$$

$$Z = \frac{z}{b},$$

$$and\ Y = \frac{y}{b}.$$

The dimensionless, steady-state, form of the conservation of energy now becomes

$$\frac{\partial^2 \theta}{\partial Y^2} + \frac{\partial^2 \theta}{\partial Z^2} = 0, \quad 0 \le Z \le \xi, \quad 0 \le Y \le 1, \tag{1a}$$

with the boundary conditions

$$\frac{d\theta}{dY} = 0, \quad Y = 0, \tag{1b}$$

$$\frac{d\theta}{dY} + Bi\theta = 0, \quad Y = 1, \tag{1c}$$

$$\frac{d\theta}{dZ} = -\eta, \quad Z = 0, \tag{1d}$$

$$\text{and } \theta = 1, \quad Z = \xi. \tag{1e}$$

The dimensionless solution of Eqs. (1a-1e) is given by

$$\theta(Z,Y) = \sum_{m=1}^{\infty} \left(\cosh(\beta_m Z) + \frac{\eta}{\beta_m} \sinh(\beta_m (\xi - Z)) \right) \left(\frac{2\cos(\beta_m Y)(\sin \beta_m)(\beta_m{}^2 + Bi^2)}{\beta_m [(\beta_m{}^2 + Bi^2) + Bi] \cosh(\beta_m \xi)} \right), \tag{2}$$

where β_ms are the positive roots of

$$\beta_m \tan(\beta_m) = Bi.$$

3.2 Cylindrical

The dimensionless, steady-state, form of the example shown in Figure1d is formulated using the dimensionless parameters

$$\theta = \frac{(T - T_\infty)}{(T_c - T_\infty)},$$

$$Z = \frac{z}{b},$$

$$and\ R = \frac{r}{b}.$$

The dimensionless form of the conservation of energy becomes

$$\frac{\partial^2\theta}{\partial R^2} + \frac{1}{R}\frac{\partial\theta}{\partial R} + \frac{\partial^2\theta}{\partial Z^2} = 0, \quad 0 \le Z \le \xi, \quad 0 \le R \le 1, \tag{3a}$$

with the boundary conditions

$$\frac{d\theta}{dR} = 0, \quad R = 0, \tag{3b}$$

$$\frac{d\theta}{dR} + Bi\theta = 0, \quad R = 1, \tag{3c}$$

$$\frac{d\theta}{dZ} = -\eta, \quad Z = 0, \tag{3d}$$

$$\text{and } \theta = 1, \quad Z = \xi. \tag{3e}$$

The dimensionless solution of Eqs. (3a-3e) is given by

$$\theta(Z,R) = \sum_{m=1}^{\infty}\left(\cosh(\beta_m Z) + \frac{\eta}{\beta_m}\sinh(\beta_m(\xi - Z))\right)\left(\frac{2BiJ_0(\beta_m R)}{J_0(\beta_m)(\beta_m{}^2 + Bi^2)\cosh(\beta_m \xi)}\right), \tag{4}$$

where β_ms are the positive roots of

$$\beta_m J_1(\beta_m) = Bi.J_0(\beta_m).$$

4.0 RESULTS

Equations 2 and 4 were solved to determine the effect on the surface temperature across the top surface at $Z = 0$ for both the rectangular and cylindrical cases. The top surface temperatures at the centerline, $\theta(0,0)$, and temperature variation, $\theta(0,0) - \theta(0,1)$, were calculated for varying dimensionless heat input, η, aspect ratio, ξ, and Biot number of the form $1/Bi$. The eigenvalues were solved using a bisection method. The number of eigenvalues, used in the series expansion, was chosen in such a manner that when doubled, the resulting solution varied less than 1%. The results of these calculations are shown, as plots, in Figs. 2-15 and Figs. 16-29 for the rectangular and cylindrical cases respectively.

There were small variations when the results for the rectangular and cylindrical cases were compared; but overall, both show the same trend as dimensionless heat input, η, aspect ratio, ξ, and Biot number of the form, $1/Bi$, were varied.

4.1 Rectangular

Figures 2-15 are grouped into three sets of plots each highlighting the effects of the three varying parameters; dimensionless heat input, η, aspect ratio, ξ, and Biot number of the form $1/Bi$. Figures 2-5 show the variation in the top surface dimensionless centerline temperature, $\theta(0,0)$, and temperature variation, $\theta(0,0) - \theta(0,1)$, plotted against $1/Bi$ with aspect ratio, ξ, varying from 0.01 to 5 and dimensionless heat input, η, varying from -0.5 to 0.5. Figures 6-10 show the variation in the top surface dimensionless centerline temperature, $\theta(0,0)$, and temperature variation, $\theta(0,0) - \theta(0,1)$, plotted against dimensionless heat input, η, with $1/Bi$ varying from 0.01 to 1000 and aspect ratio, ξ, varying from 0.25 to 5. Figures 11-15 show the variation in the top surface dimensionless centerline temperature, $\theta(0,0)$, and temperature variation, $\theta(0,0) - \theta(0,1)$, plotted against aspect ratio, ξ, with $1/Bi$ varying from 0.01 to 1000 and dimensionless heat input, η, varying from -0.5 to 0.5.

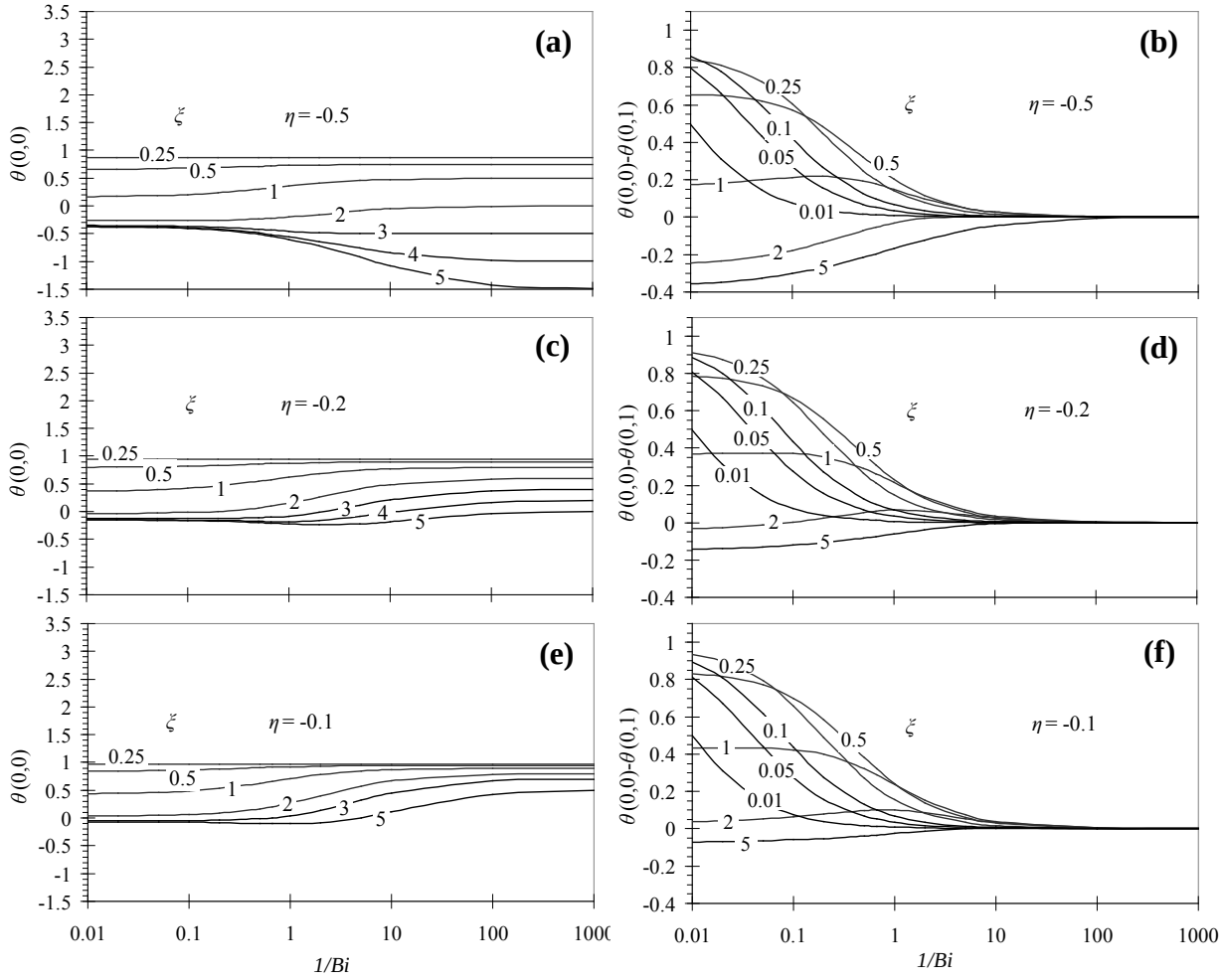

Figure 2. Top surface dimensionless centerline temperature, $\theta(0,0)$, and temperature variation, $\theta(0,0) - \theta(0,1)$, plotted against $1/Bi$ for varying aspect ratio, ξ; (a), (b) η = -0.5, (c), (d) η = -0.2, and (e), (f) η = -0.1.

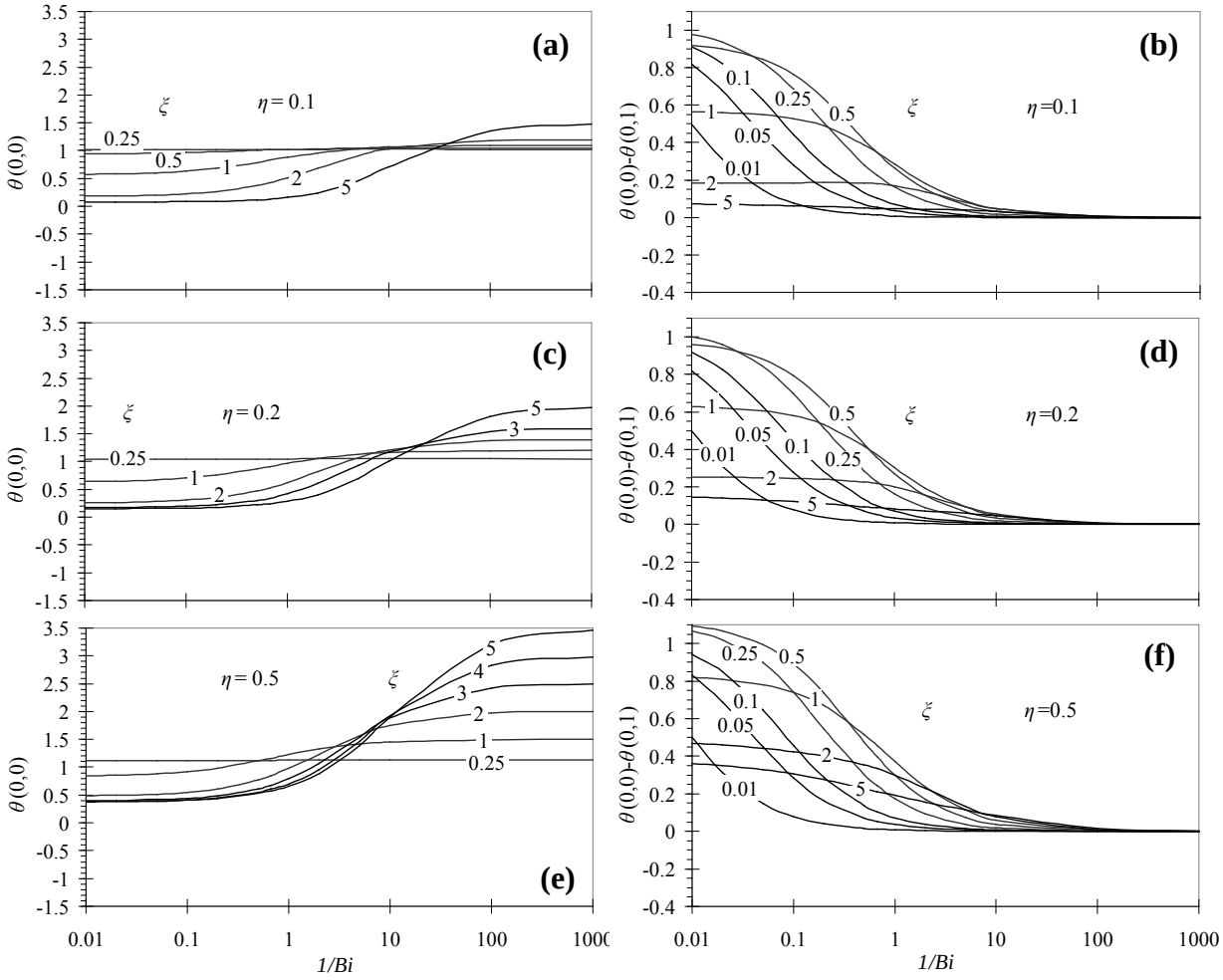

Figure 3. Top surface dimensionless centerline temperature, $\theta(0,0)$, and temperature variation, $\theta(0,0) - \theta(0,1)$, plotted against $1/Bi$ for varying aspect ratio, ξ; (a), (b) $\eta = 0.1$, (c), (d) $\eta = 0.2$, and (e), (f) $\eta = 0.5$.

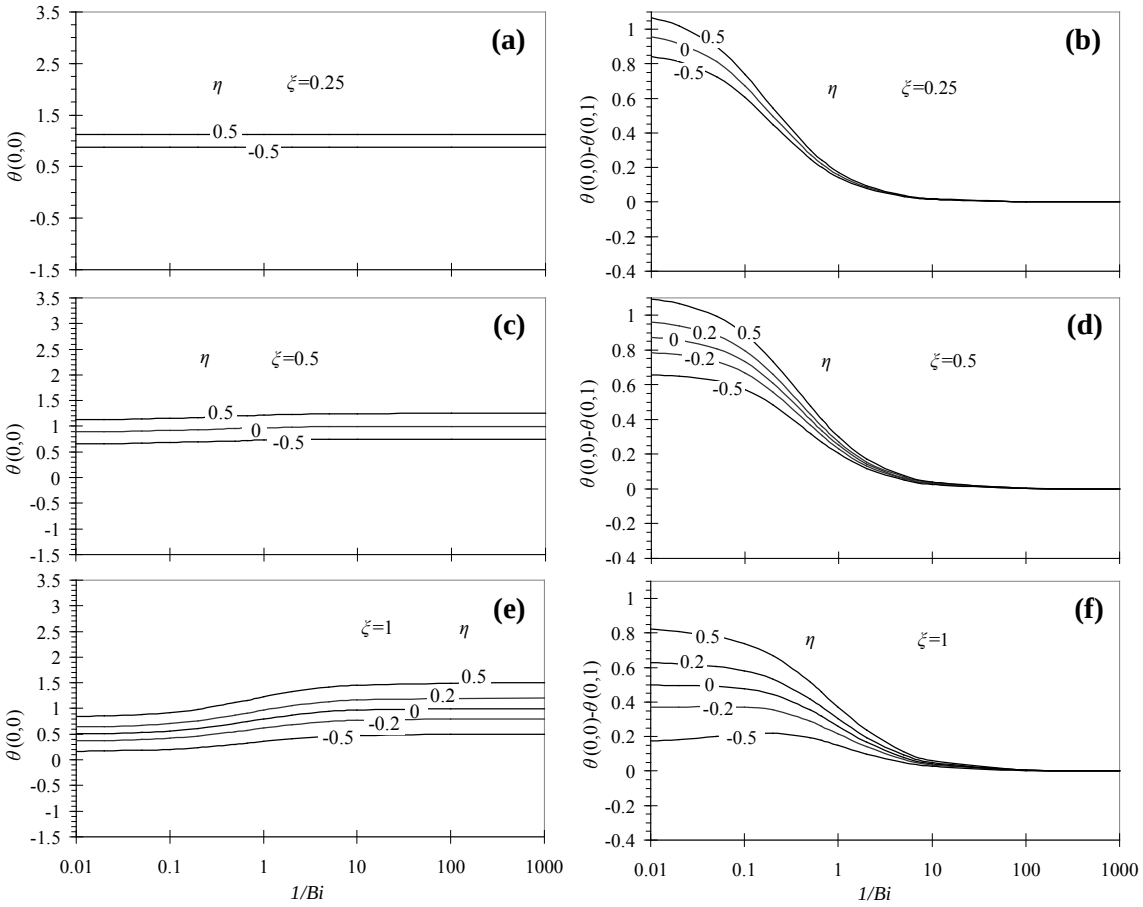

Figure 4. Top surface dimensionless centerline temperature, $\theta(0,0)$, and temperature variation, $\theta(0,0) - \theta(0,1)$, plotted against $1/Bi$ for varying dimensionless heat input, η; (a), (b) $\xi = 0.25$, (c), (d) $\xi = 0.5$, and (e), (f) $\xi = 1$.

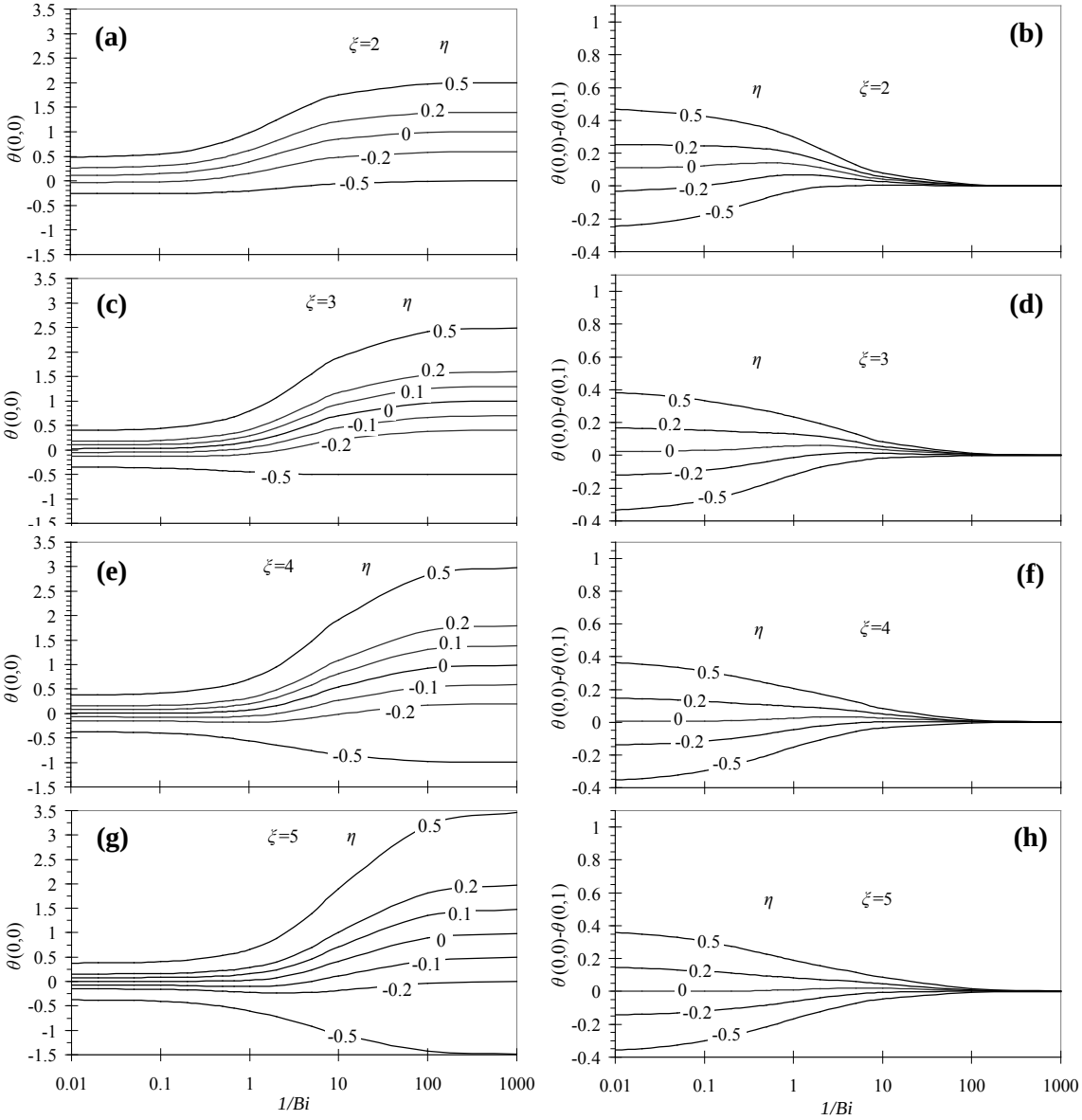

Figure 5. Top surface dimensionless centerline temperature, $\theta(0,0)$, and temperature variation, $\theta(0,0) - \theta(0,1)$, plotted against $1/Bi$ for varying dimensionless heat input, η; (a), (b) $\xi = 2$, (c), (d) $\xi = 3$, (e), (f) $\xi = 4$, and (g), (h) $\xi = 5$.

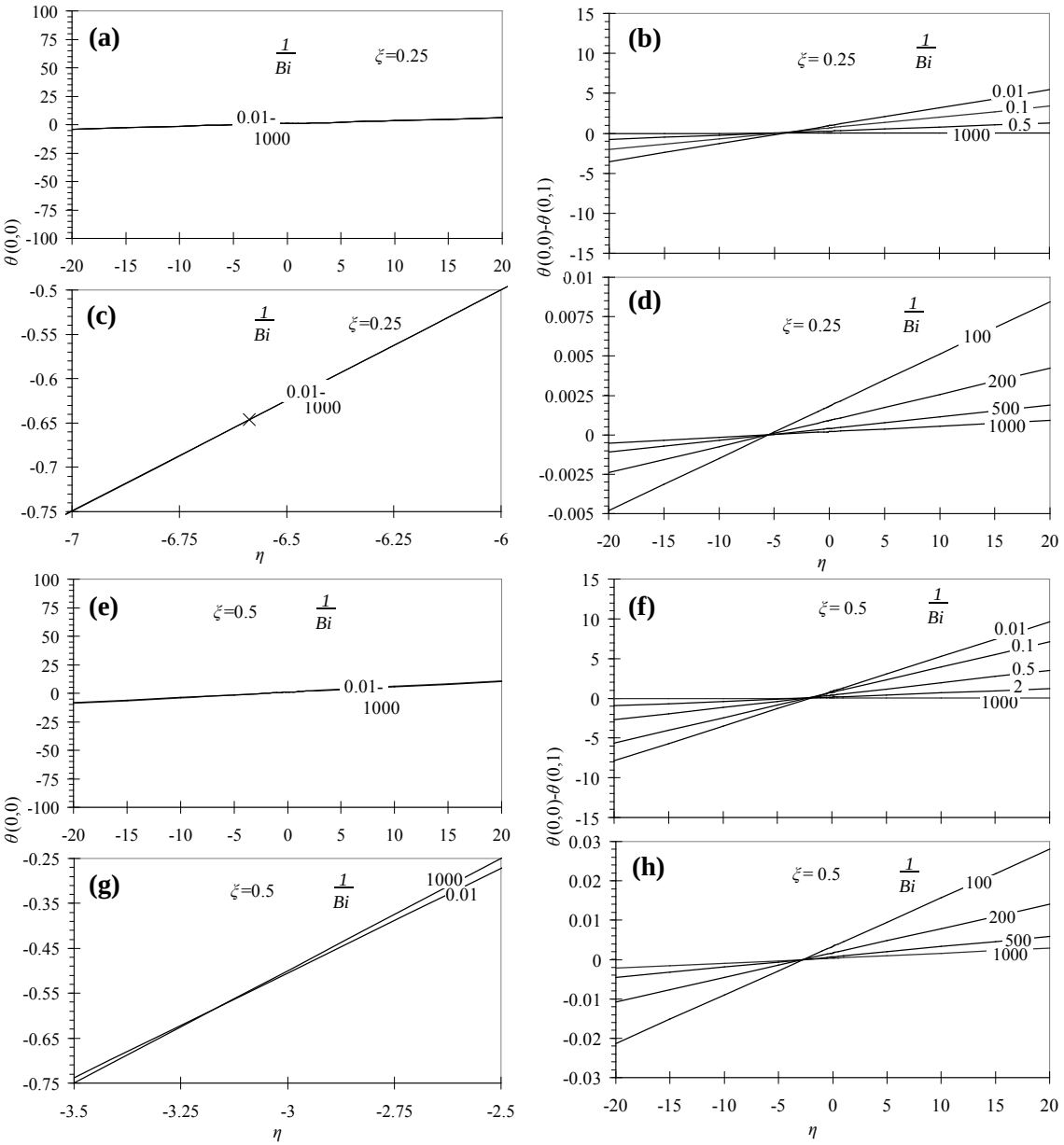

Figure 6. Top surface dimensionless centerline temperature, $\theta(0,0)$, and temperature variation, $\theta(0,0) - \theta(0,1)$, plotted against dimensionless heat input, η, for varying $1/Bi$; (a), (b), (c), (d) $\xi = 0.25$ and (e), (f), (g), (h) $\xi = 0.5$.

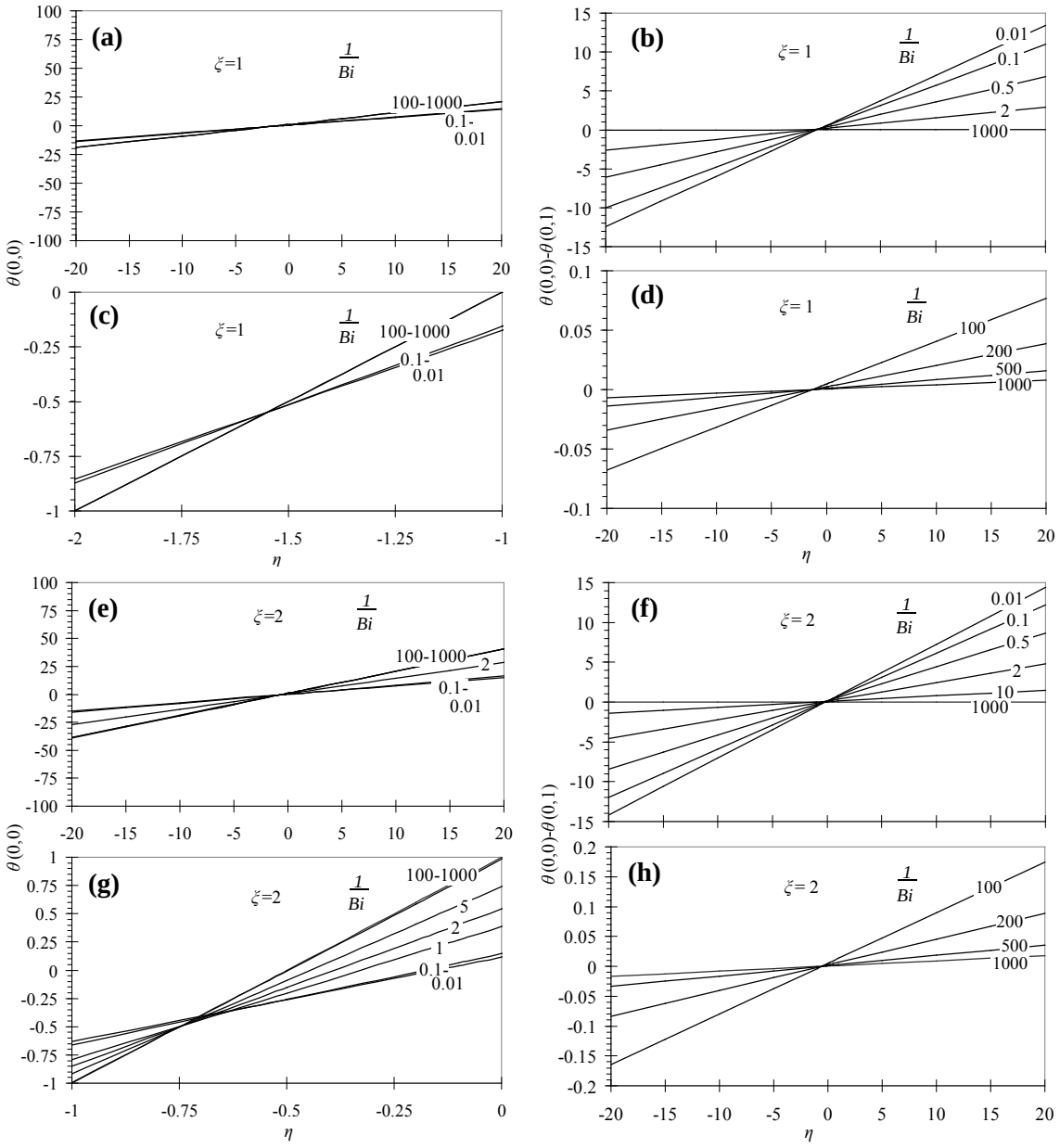

Figure 7. Top surface dimensionless centerline temperature, $\theta(0,0)$, and temperature variation, $\theta(0,0) - \theta(0,1)$, plotted against dimensionless heat input, η, for varying $1/Bi$; (a), (b), (c), (d) $\xi = 1$ and (e), (f), (g), (h) $\xi = 2$.

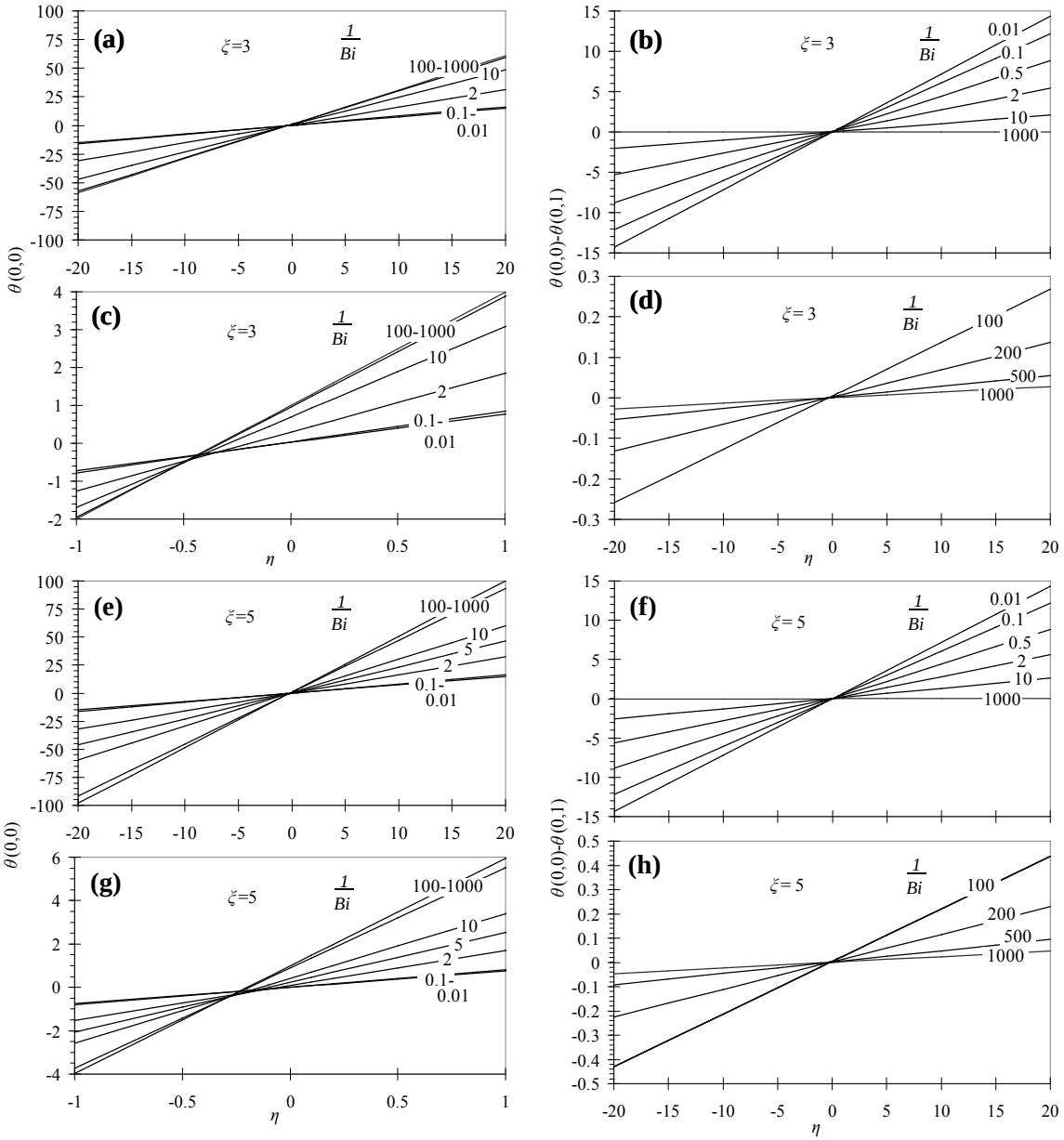

Figure 8. Top surface dimensionless centerline temperature, $\theta(0,0)$, and temperature variation, $\theta(0,0) - \theta(0,1)$, plotted against dimensionless heat input, η, for varying $1/Bi$; (a), (b), (c), (d) $\xi = 3$ and (e), (f), (g), (h) $\xi = 5$.

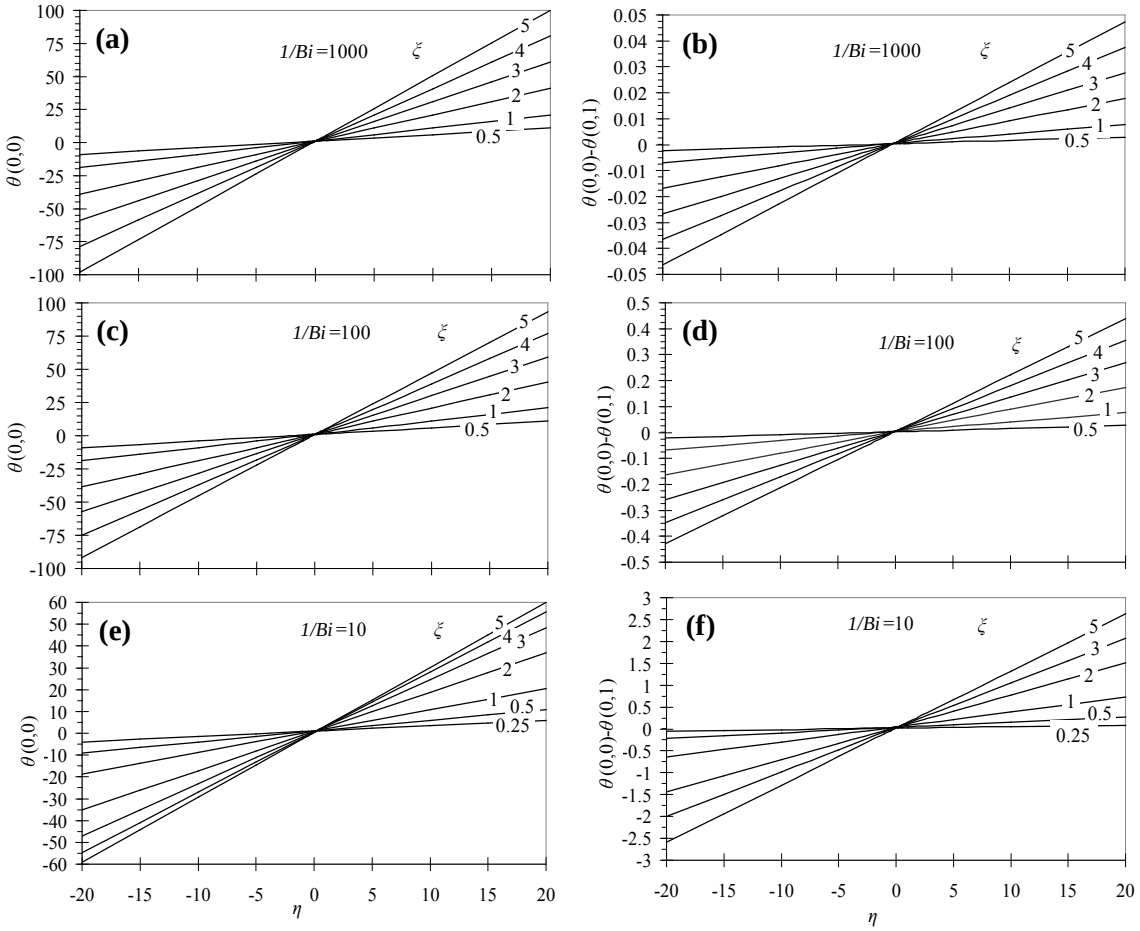

Figure 9. Top surface dimensionless centerline temperature, $\theta(0,0)$, and temperature variation, $\theta(0,0) - \theta(0,1)$, plotted against dimensionless heat input, η, for varying aspect ratio, ξ; (a), (b) $1/Bi = 1000$, (c), (d) $1/Bi = 100$, and (e), (f) $1/Bi = 10$.

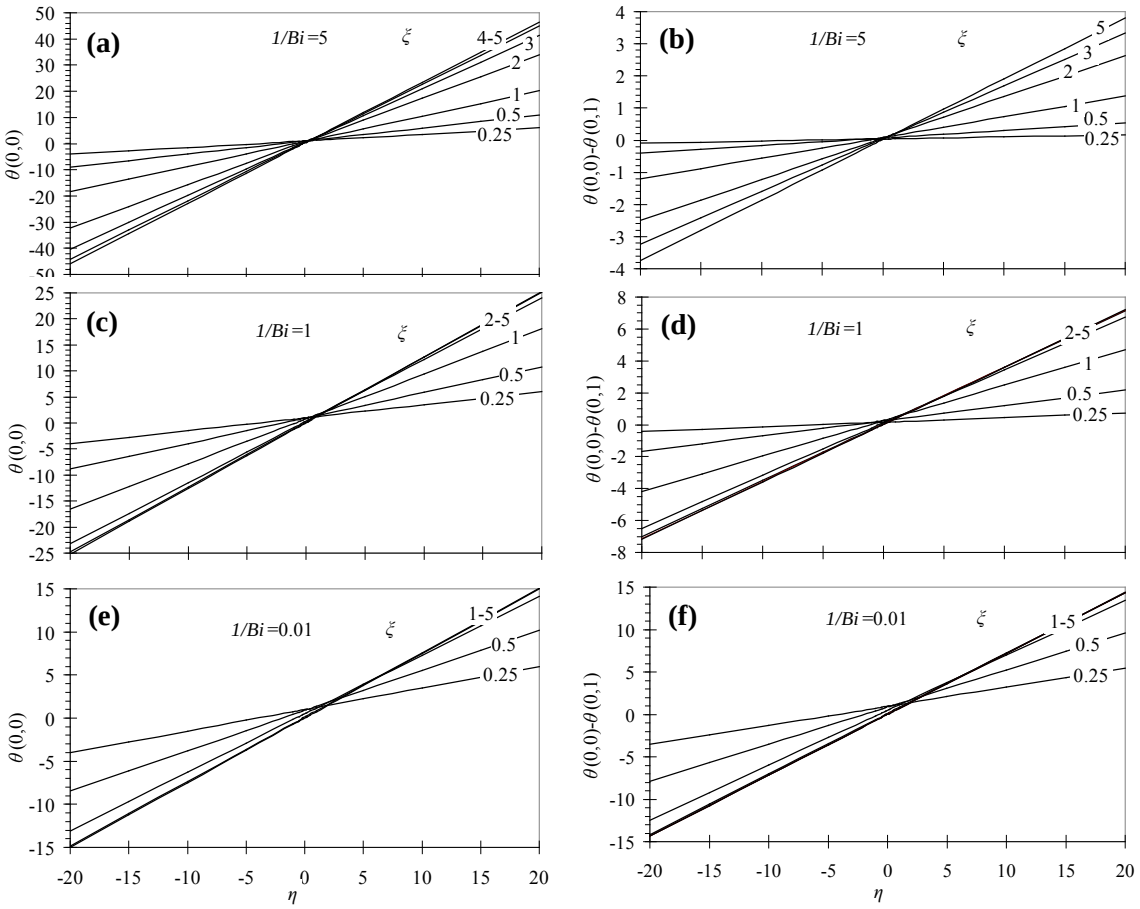

Figure 10. Top surface dimensionless centerline temperature, $\theta(0,0)$, and temperature variation, $\theta(0,0) - \theta(0,1)$, plotted against dimensionless heat input, η, for varying aspect ratio, ξ; (a), (b) $1/Bi = 5$, (c), (d) $1/Bi = 1$, and (e), (f) $1/Bi = 0.01$.

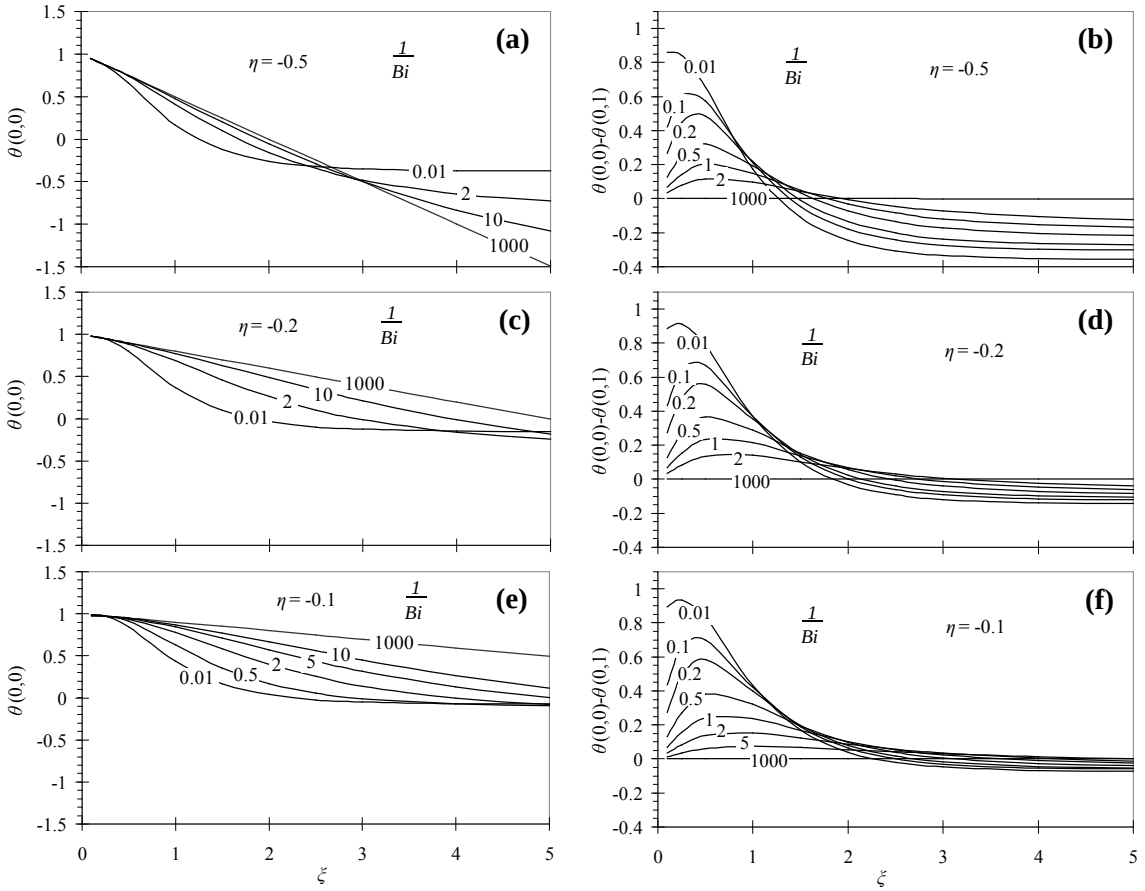

Figure 11. Top surface dimensionless centerline temperature, $\theta(0,0)$, and temperature variation, $\theta(0,0) - \theta(0,1)$, plotted against aspect ratio, ξ, for varying $1/Bi$; (a), (b) η = -0.5, (c), (d) η = -0.2, and (e), (f) η = -0.1.

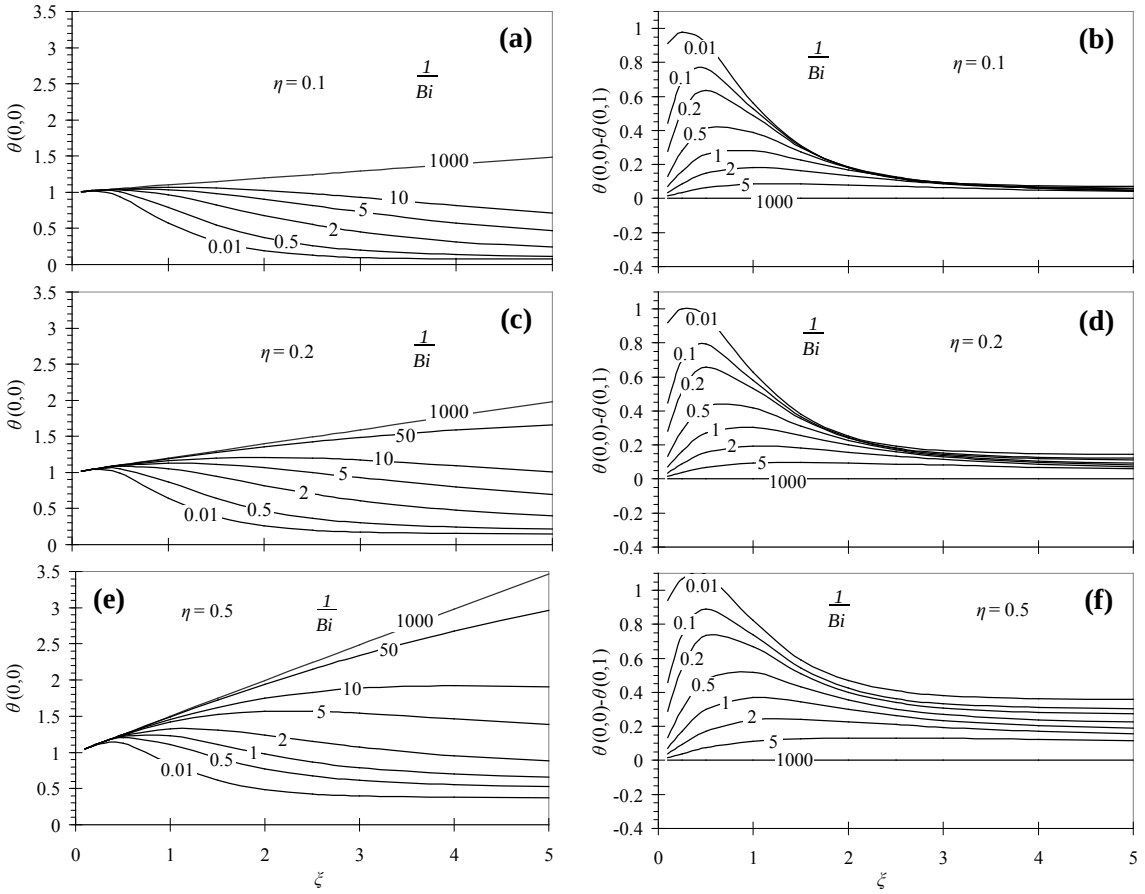

Figure 12. Top surface dimensionless centerline temperature, $\theta(0,0)$, and temperature variation, $\theta(0,0) - \theta(0,1)$, plotted against aspect ratio, ξ, for varying $1/Bi$; (a), (b) $\eta = 0.1$, (c), (d) $\eta = 0.2$, and (e), (f) $\eta = 0.5$.

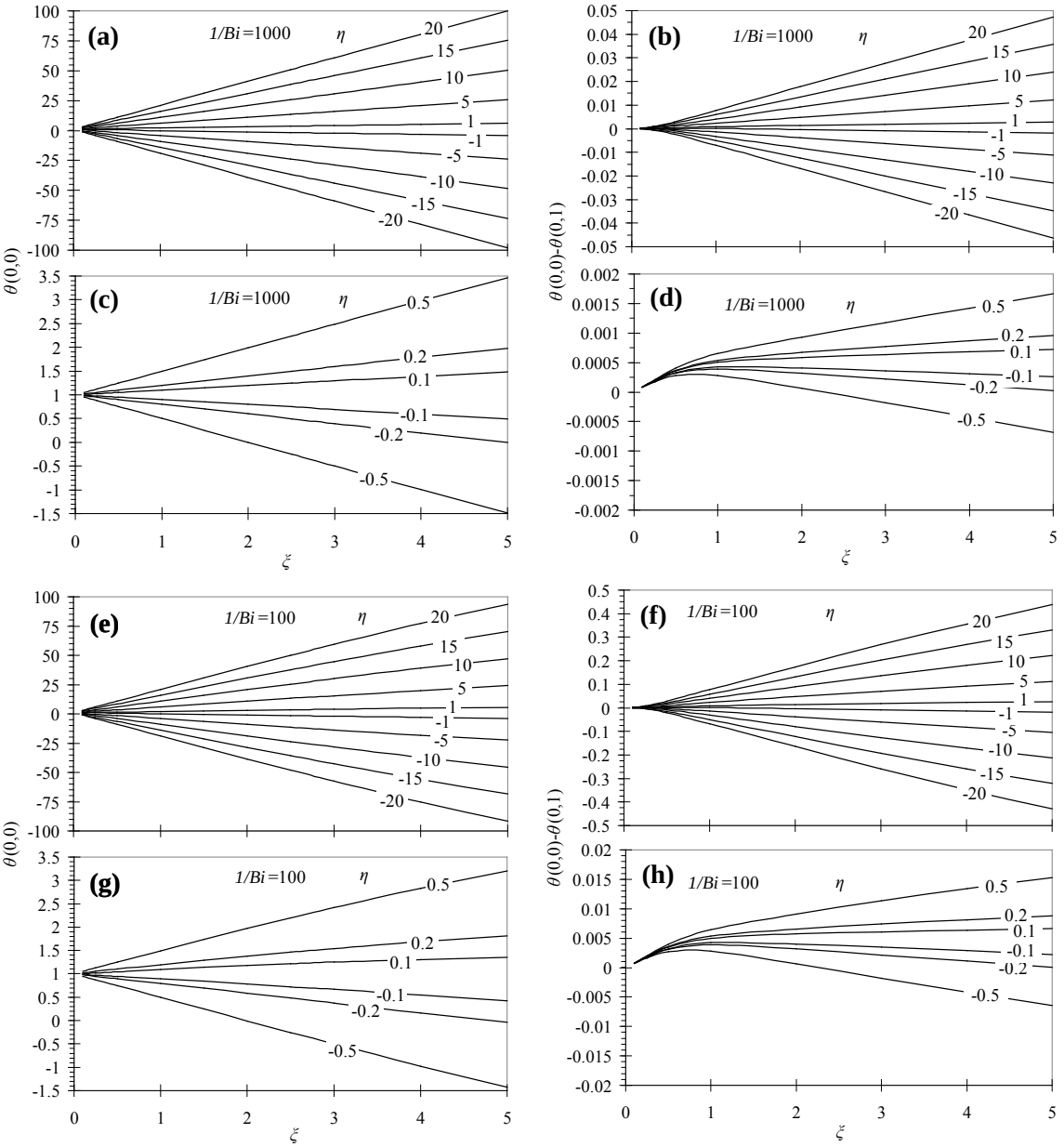

Figure 13. Top surface dimensionless centerline temperature, $\theta(0,0)$, and temperature variation, $\theta(0,0) - \theta(0,1)$, plotted against aspect ratio, ξ, for varying dimensionless heat input, η; (a), (b), (c), (d) $1/Bi$ = 1000 and (e), (f), (g), (h) $1/Bi$ = 100.

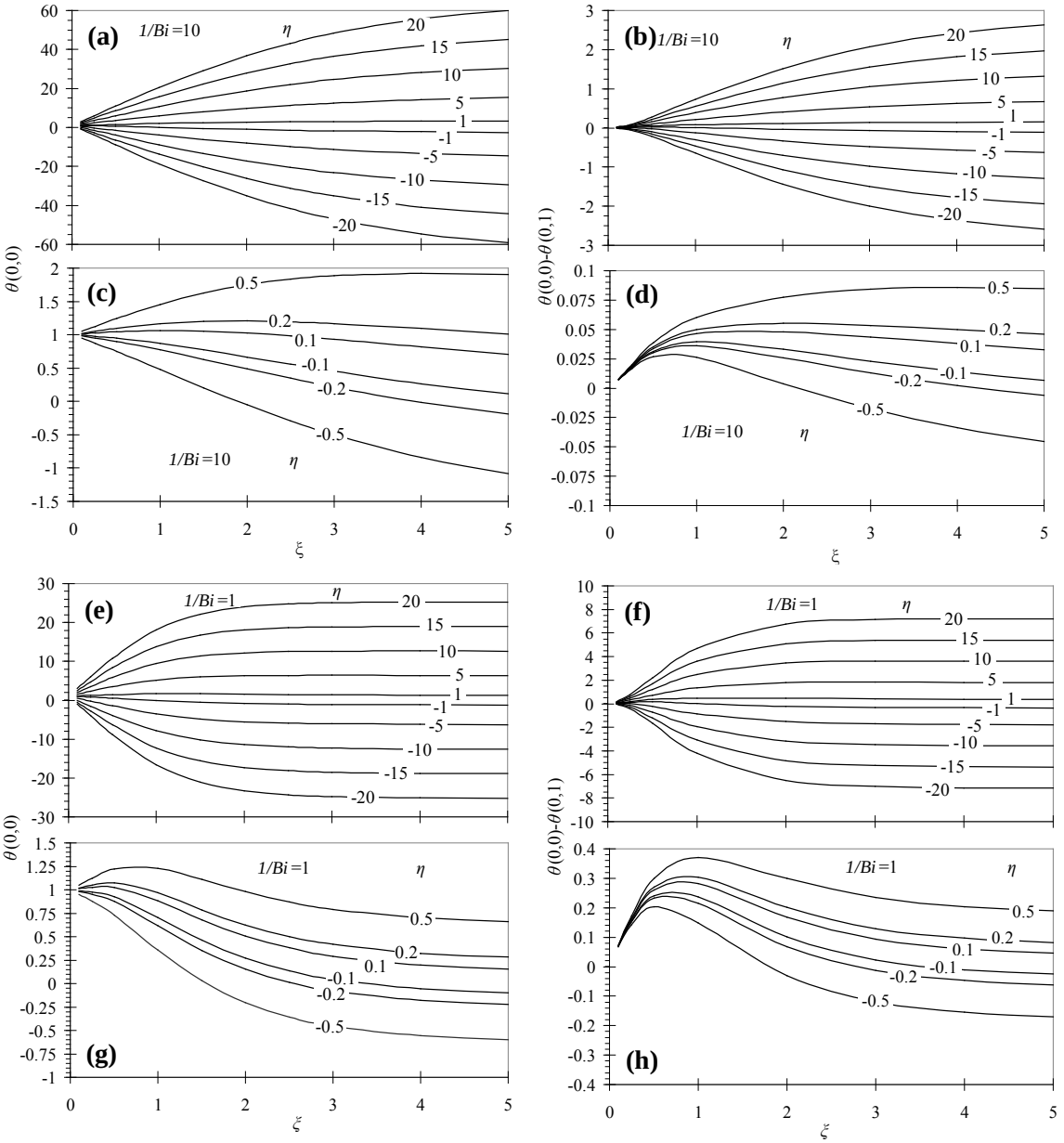

Figure 14. Top surface dimensionless centerline temperature, $\theta(0,0)$, and temperature variation, $\theta(0,0) - \theta(0,1)$, plotted against aspect ratio, ξ, for varying dimensionless heat input, η; (a), (b), (c), (d) $1/Bi = 10$ and (e), (f), (g), (h) $1/Bi = 1$.

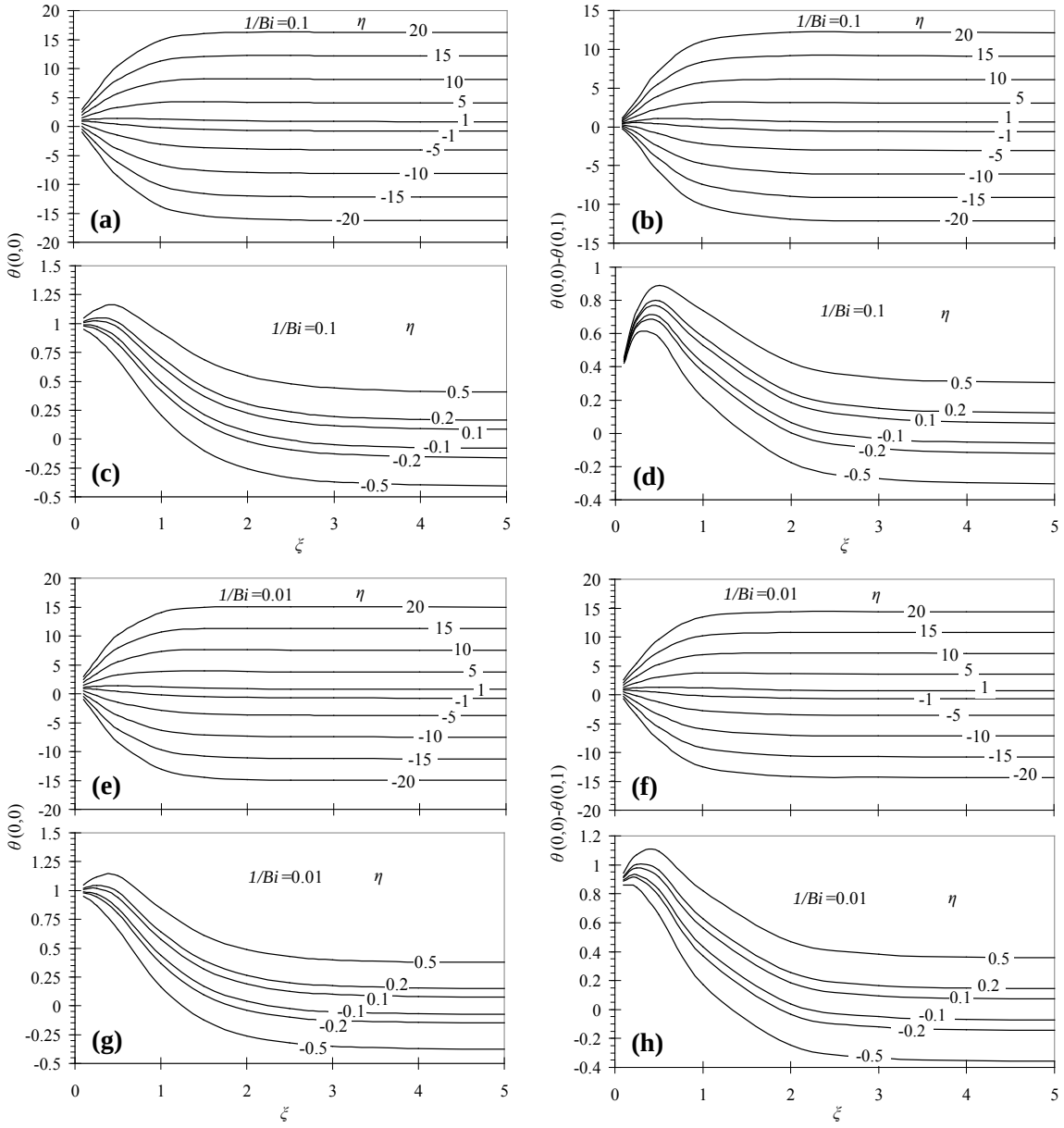

Figure 15. Top surface dimensionless centerline temperature, $\theta(0,0)$, and temperature variation, $\theta(0,0) - \theta(0,1)$, plotted against aspect ratio, ξ, for varying dimensionless heat input, η; (a), (b), (c), (d) $1/Bi = 0.1$ and (e), (f), (g), (h) $1/Bi = 0.01$.

4.2 Cylindrical

Similar to the rectangular coordinate case, Figs. 16-29 are grouped into three sets of plots each highlighting the effects of the three varying parameters; dimensionless heat input, η, aspect ratio, ξ, and Biot number of the form $1/Bi$. Figures 16-19 show the variation in the top surface dimensionless centerline temperature, $\theta(0,0)$, and temperature variation, $\theta(0,0) - \theta(0,1)$, plotted against $1/Bi$ with aspect ratio, ξ, varying from 0.01 to 5 and dimensionless heat input, η, varying from -0.5 to 0.5. Figures 20-24 show the variation in the top surface dimensionless centerline temperature, $\theta(0,0)$, and temperature variation, $\theta(0,0) - \theta(0,1)$, plotted against dimensionless heat input, η, with $1/Bi$ varying from 0.01 to 1000 and aspect ratio, ξ, varying from 0.25 to 5. Figures 25-29 show the variation in the top surface dimensionless centerline temperature, $\theta(0,0)$, and temperature variation, $\theta(0,0) - \theta(0,1)$, plotted against aspect ratio, ξ, with $1/Bi$ varying from 0.01 to 1000 and dimensionless heat input, η, varying from -0.5 to 0.5.

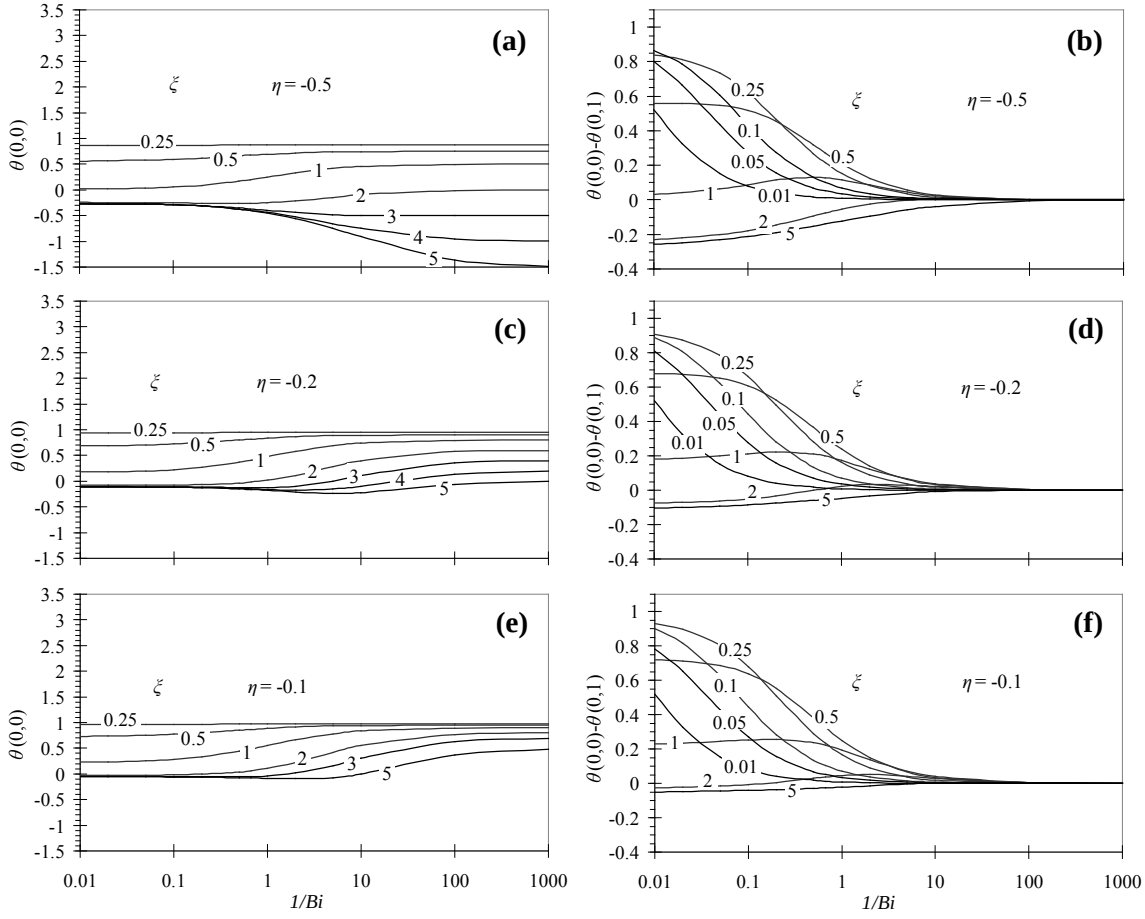

Figure 16. Top surface dimensionless centerline temperature, $\theta(0,0)$, and temperature variation, $\theta(0,0) - \theta(0,1)$, plotted against $1/Bi$ for varying aspect ratio, ξ; (a), (b) η = -0.5, (c), (d) η = -0.2, and (e), (f) η = -0.1.

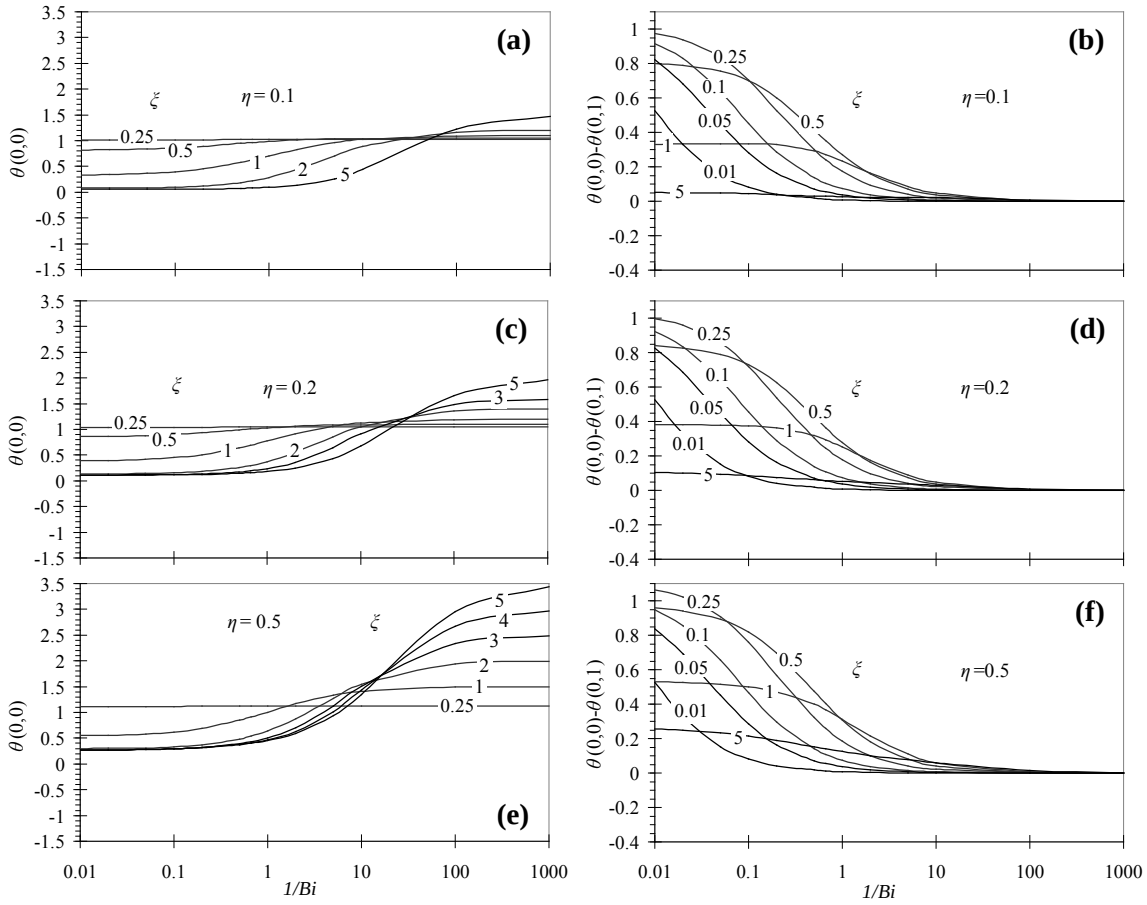

Figure 17. Top surface dimensionless centerline temperature, $\theta(0,0)$, and temperature variation, $\theta(0,0) - \theta(0,1)$, plotted against $1/Bi$ for varying aspect ratio, ξ; (a), (b) $\eta = 0.1$, (c), (d) $\eta = 0.2$, and (e), (f) $\eta = 0.5$.

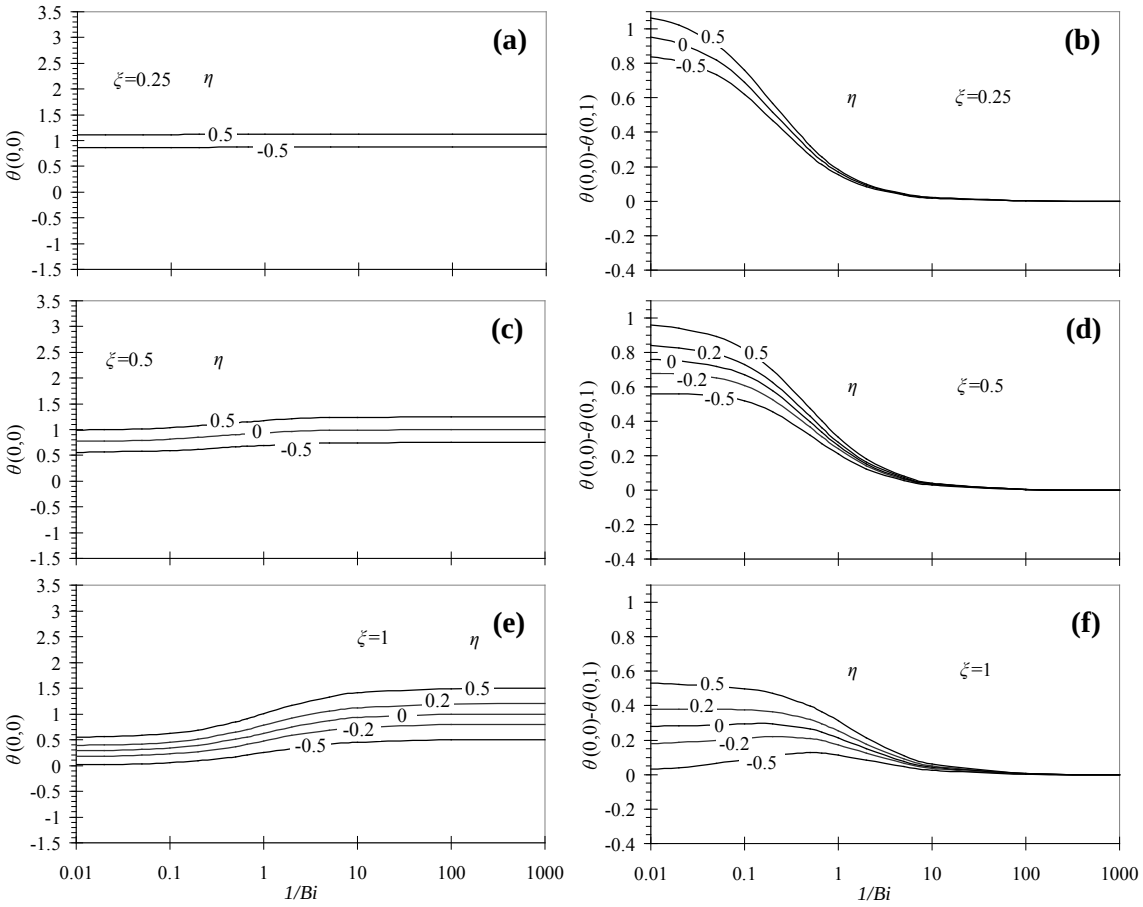

Figure 18. Top surface dimensionless centerline temperature, $\theta(0,0)$, and temperature variation, $\theta(0,0) - \theta(0,1)$, plotted against $1/Bi$ for varying dimensionless heat input, η; (a), (b) $\xi = 0.25$, (c), (d) $\xi = 0.5$, and (e), (f) $\xi = 1$.

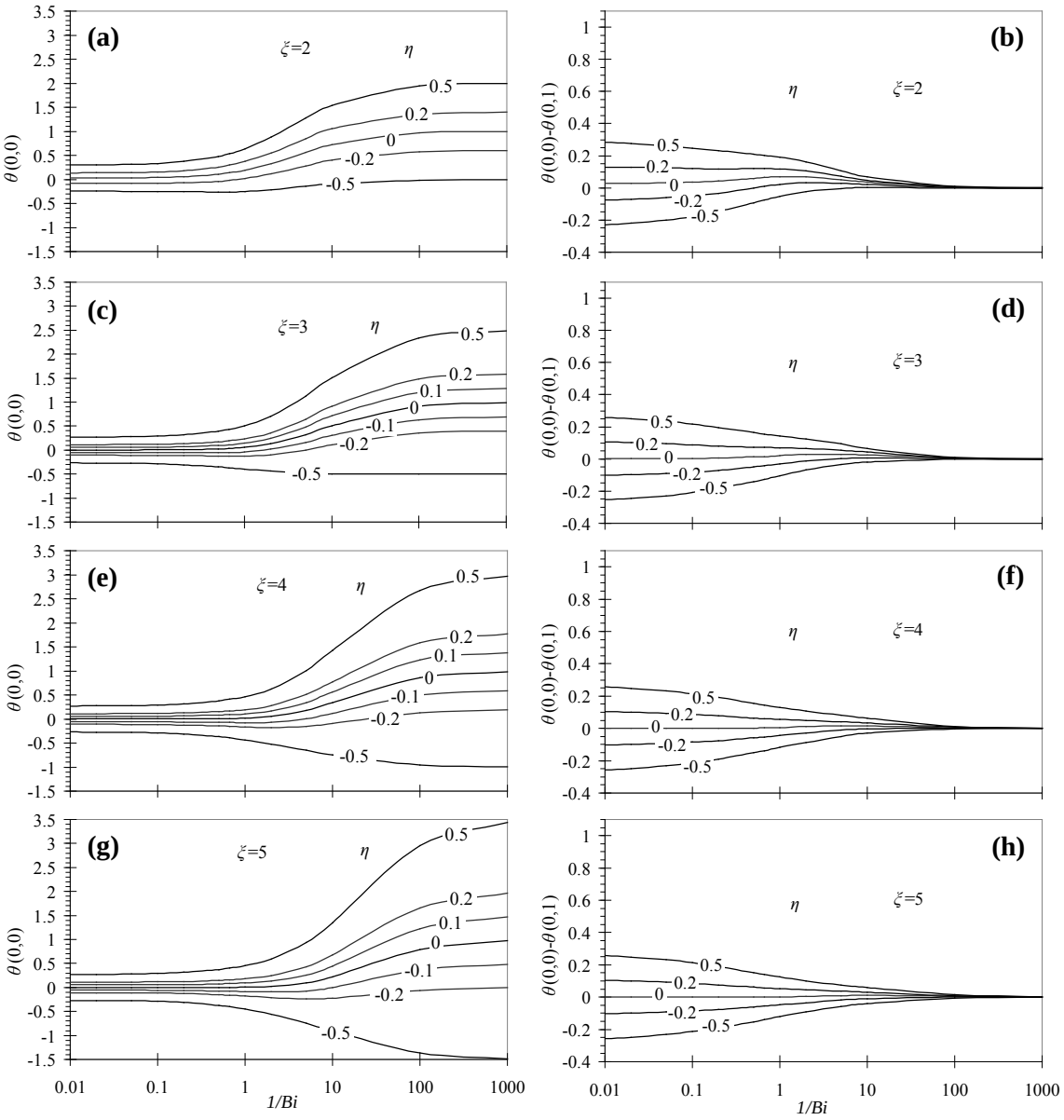

Figure 19. Top surface dimensionless centerline temperature, $\theta(0,0)$, and temperature variation, $\theta(0,0) - \theta(0,1)$, plotted against $1/Bi$ for varying dimensionless heat input, η; (a), (b) $\xi = 2$, (c), (d) $\xi = 3$, (e), (f) $\xi = 4$, and (g), (h) $\xi = 5$.

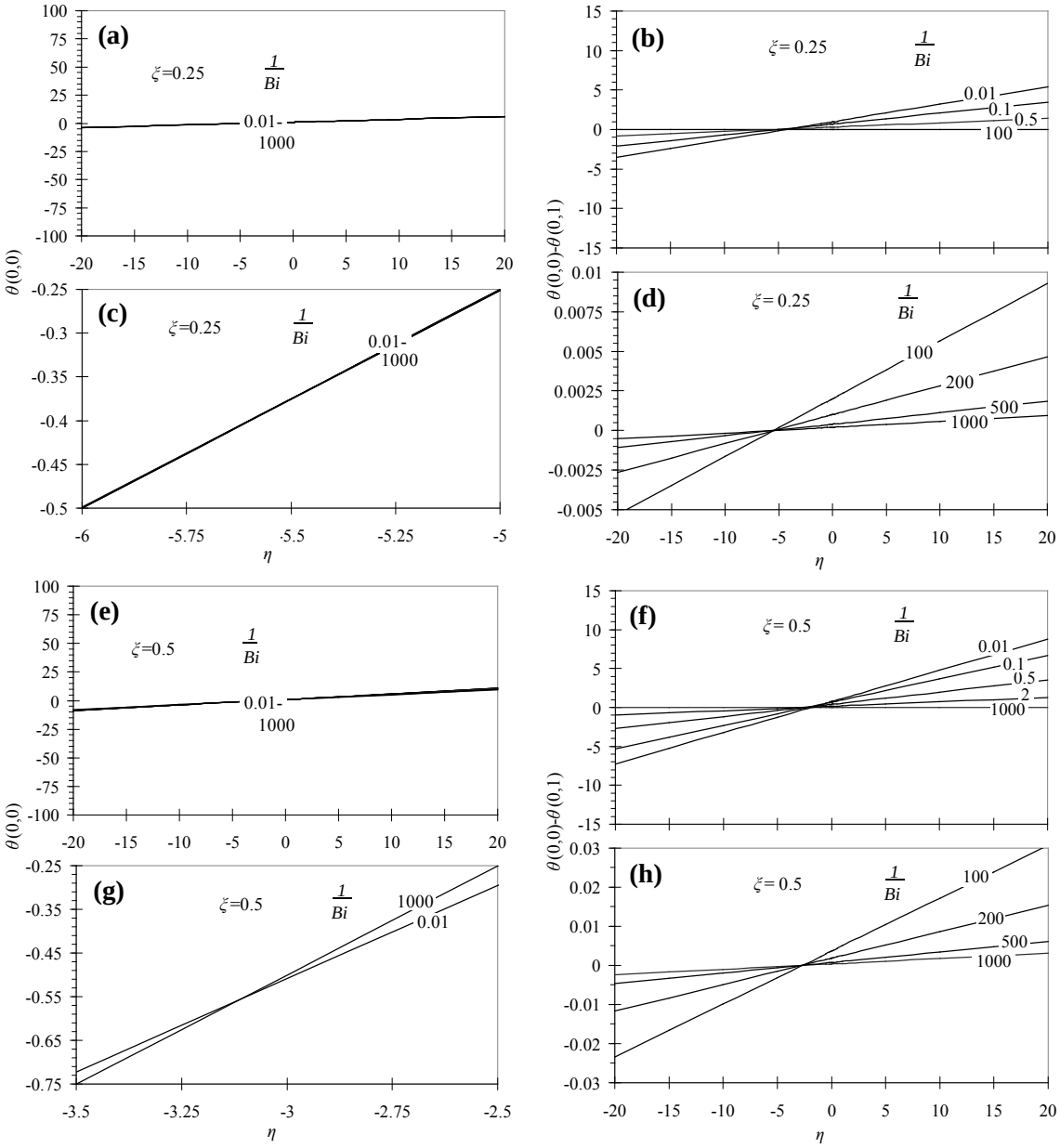

Figure 20. Top surface dimensionless centerline temperature, $\theta(0,0)$, and temperature variation, $\theta(0,0) - \theta(0,1)$, plotted against dimensionless heat input, η, for varying $1/Bi$; (a), (b), (c), (d) $\xi = 0.25$ and (e), (f), (g), (h) $\xi = 0.5$.

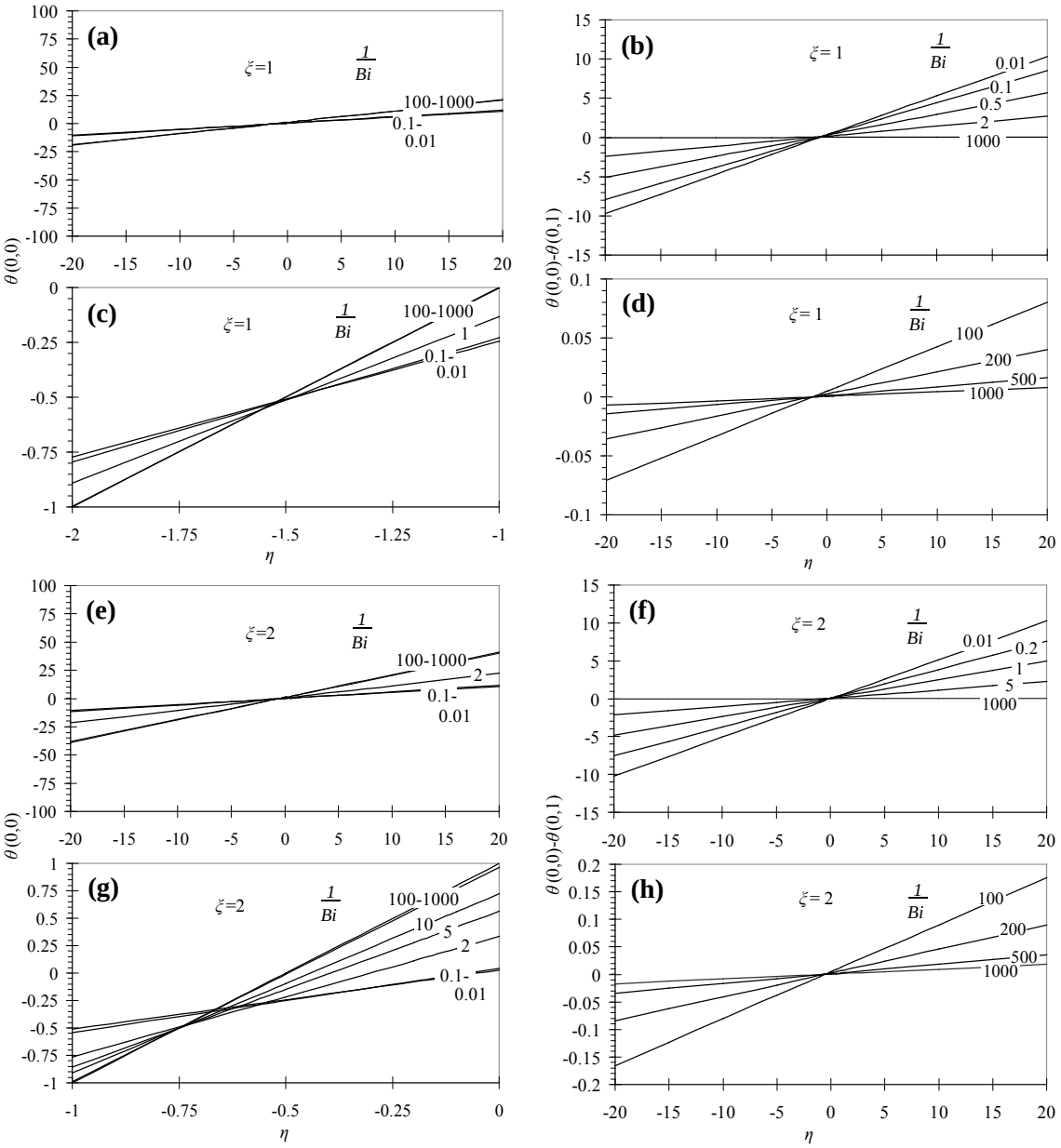

Figure 21. Top surface dimensionless centerline temperature, $\theta(0,0)$, and temperature variation, $\theta(0,0) - \theta(0,1)$, plotted against dimensionless heat input, η, for varying $1/Bi$; (a), (b), (c), (d) $\xi = 1$ and (e), (f), (g), (h) $\xi = 2$.

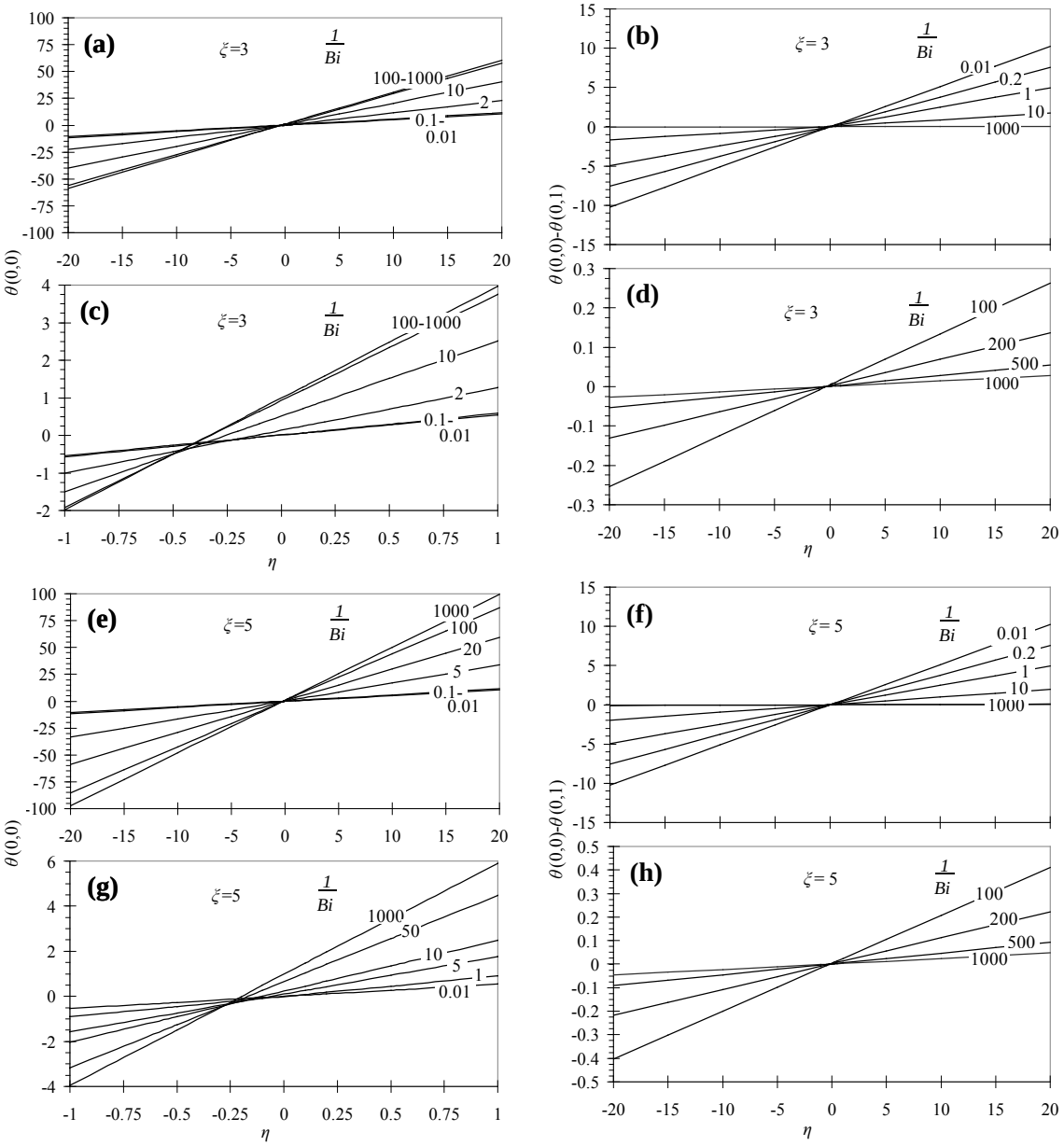

Figure 22. Top surface dimensionless centerline temperature, $\theta(0,0)$, and temperature variation, $\theta(0,0) - \theta(0,1)$, plotted against dimensionless heat input, η, for varying $1/Bi$; (a), (b), (c), (d) $\xi = 3$ and (e), (f), (g), (h) $\xi = 5$.

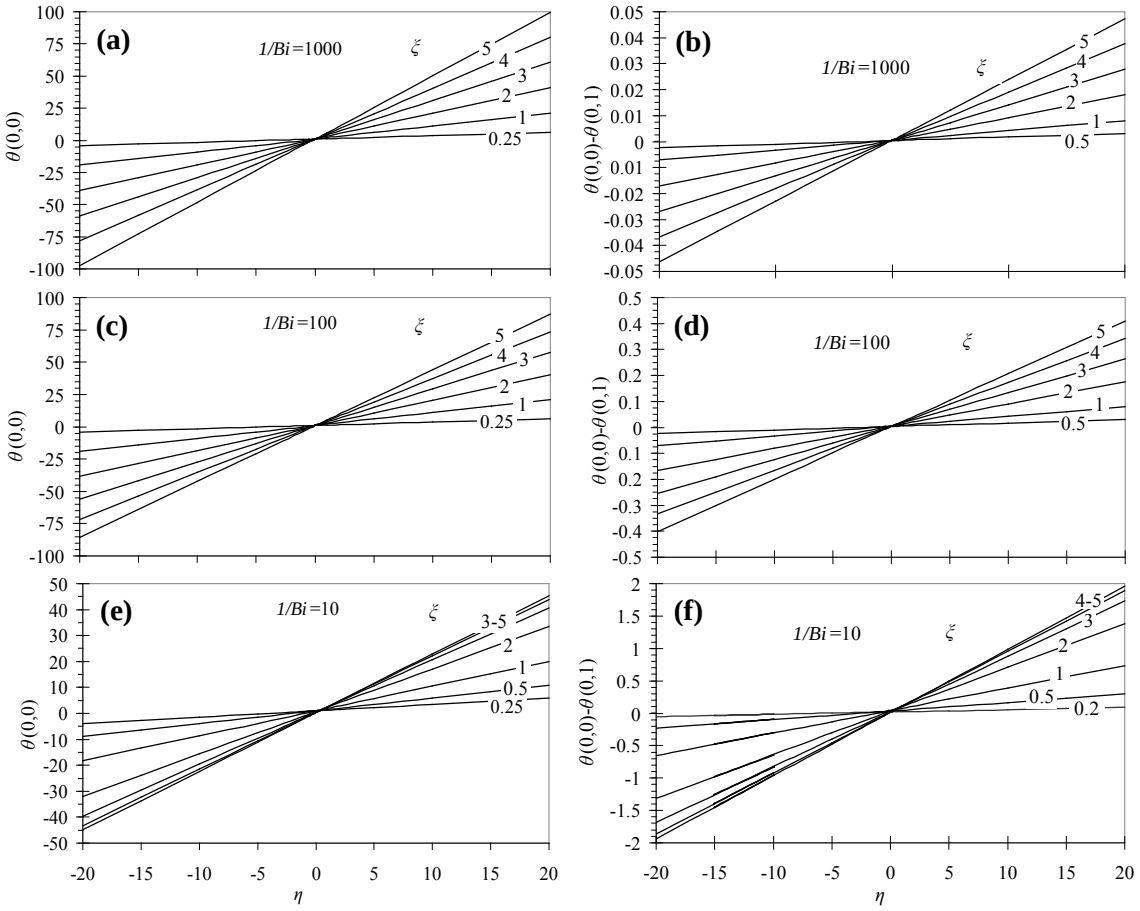

Figure 23. Top surface dimensionless centerline temperature, $\theta(0,0)$, and temperature variation, $\theta(0,0) - \theta(0,1)$, plotted against dimensionless heat input, η, for varying aspect ratio, ξ; (a), (b) $1/Bi = 1000$, (c), (d) $1/Bi = 100$, and (e), (f) $1/Bi = 10$.

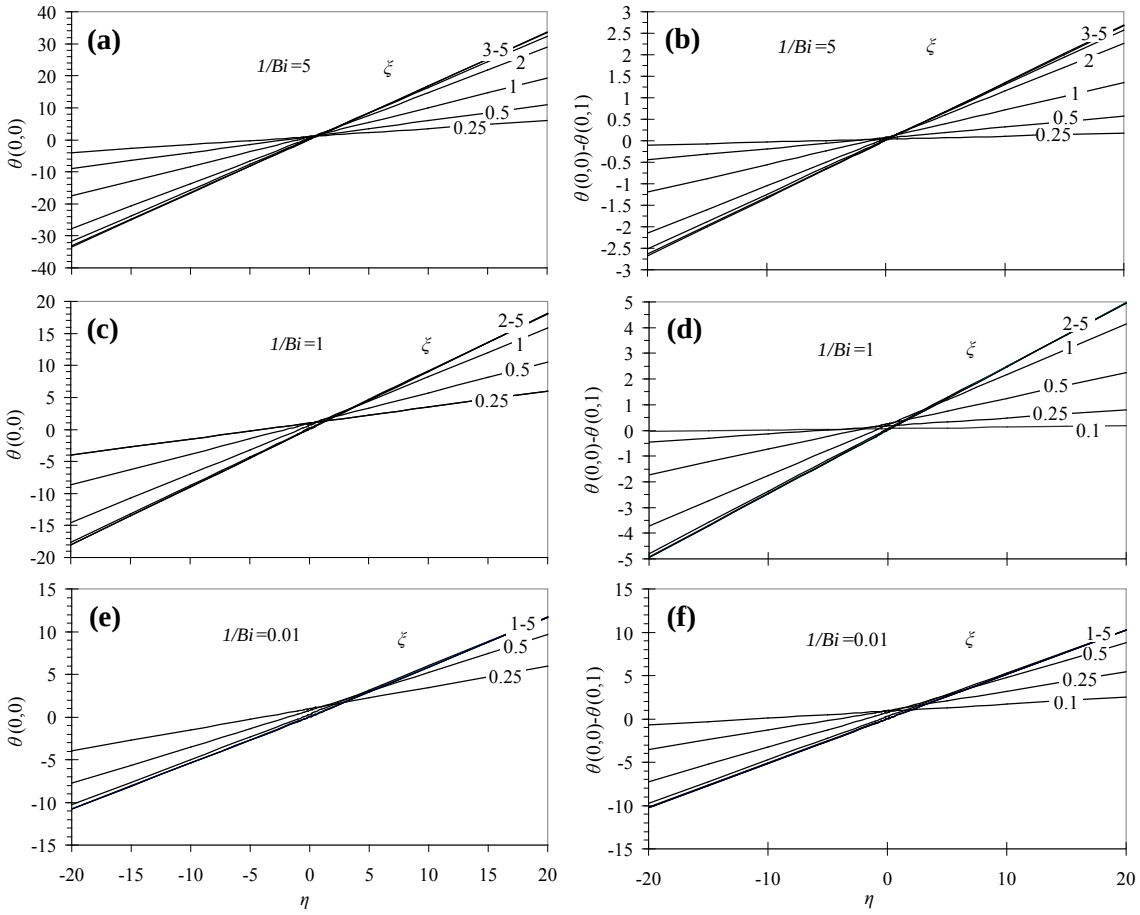

Figure 24. Top surface dimensionless centerline temperature, $\theta(0,0)$, and temperature variation, $\theta(0,0) - \theta(0,1)$, plotted against dimensionless heat input, η, for varying aspect ratio, ξ; (a), (b) $1/Bi = 5$, (c), (d) $1/Bi = 1$, and (e), (f) $1/Bi = 0.01$.

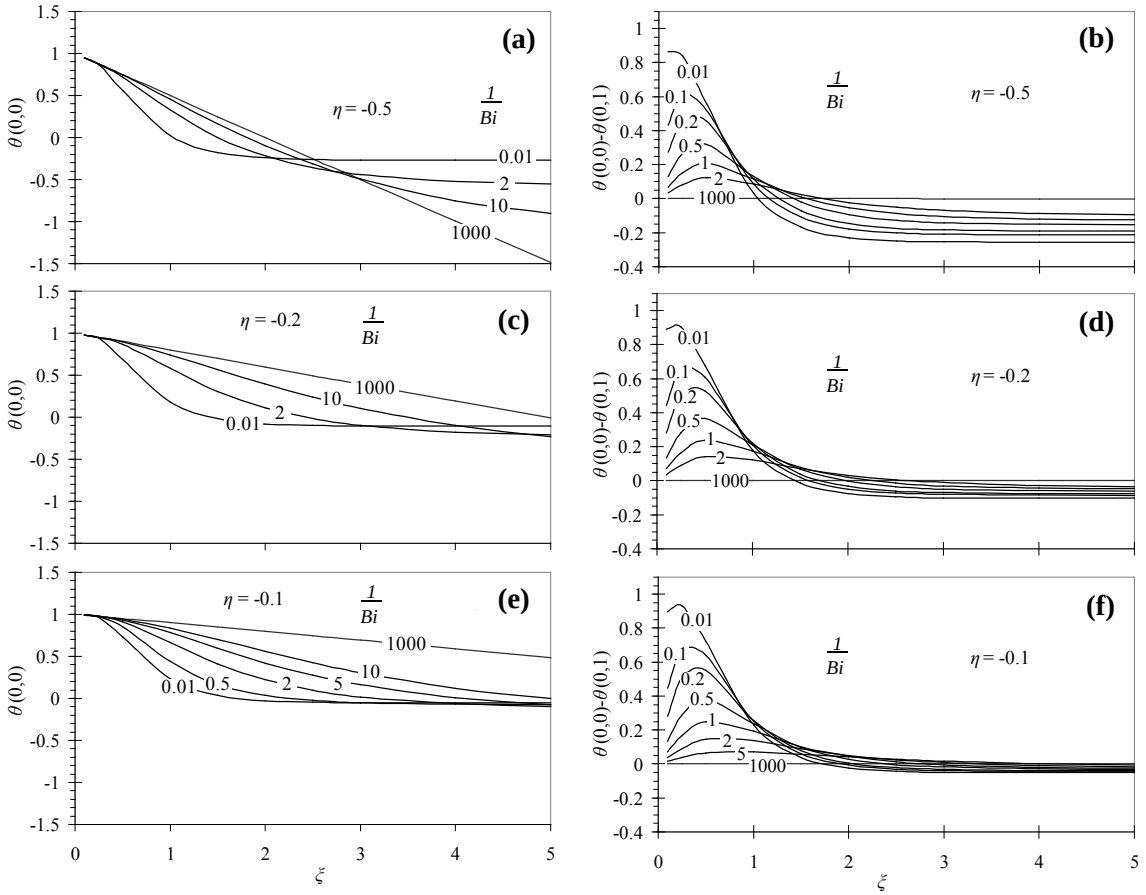

Figure 25. Top surface dimensionless centerline temperature, $\theta(0,0)$, and temperature variation, $\theta(0,0) - \theta(0,1)$, plotted against aspect ratio, ξ, for varying $1/Bi$; (a), (b) η = -0.5, (c), (d) η = -0.2, and (e), (f) η = -0.1.

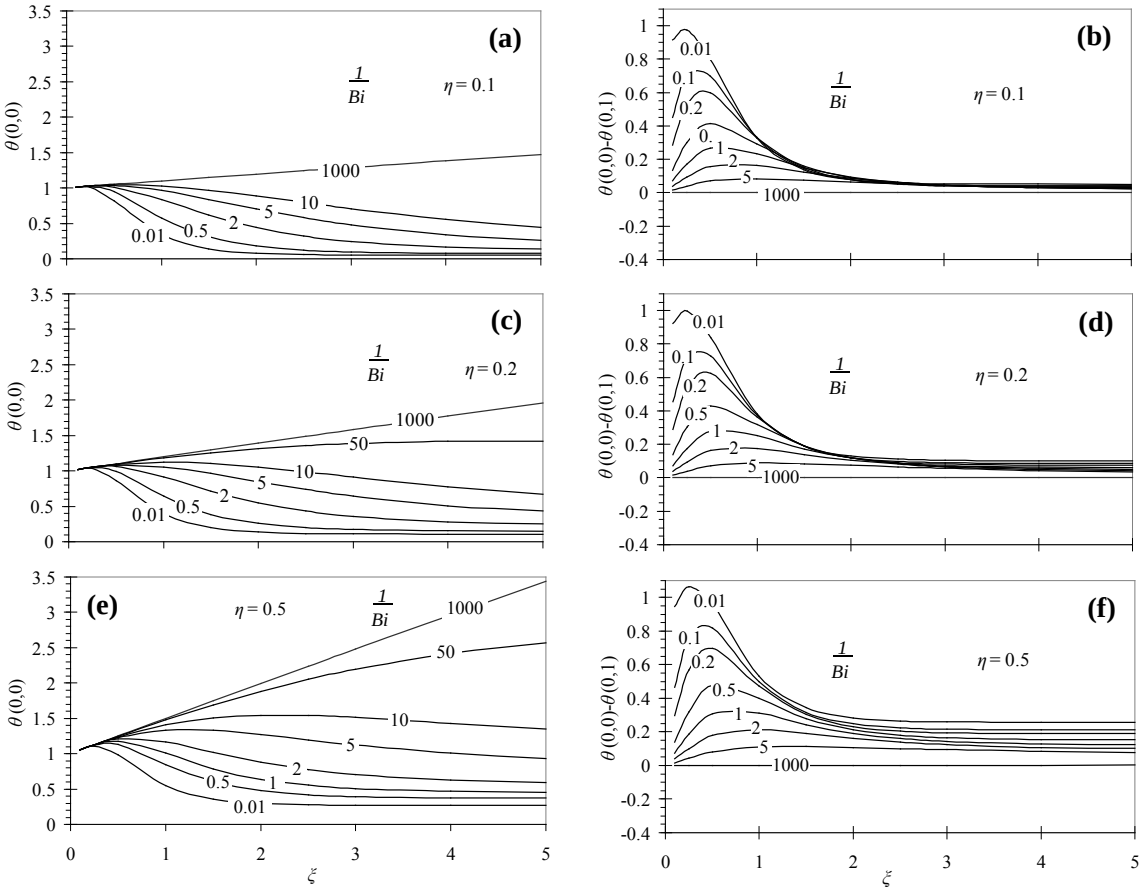

Figure 26. Top surface dimensionless centerline temperature, $\theta(0,0)$, and temperature variation, $\theta(0,0) - \theta(0,1)$, plotted against aspect ratio, ξ, for varying $1/Bi$; (a), (b) $\eta = 0.1$, (c), (d) $\eta = 0.2$, and (e), (f) $\eta = 0.5$.

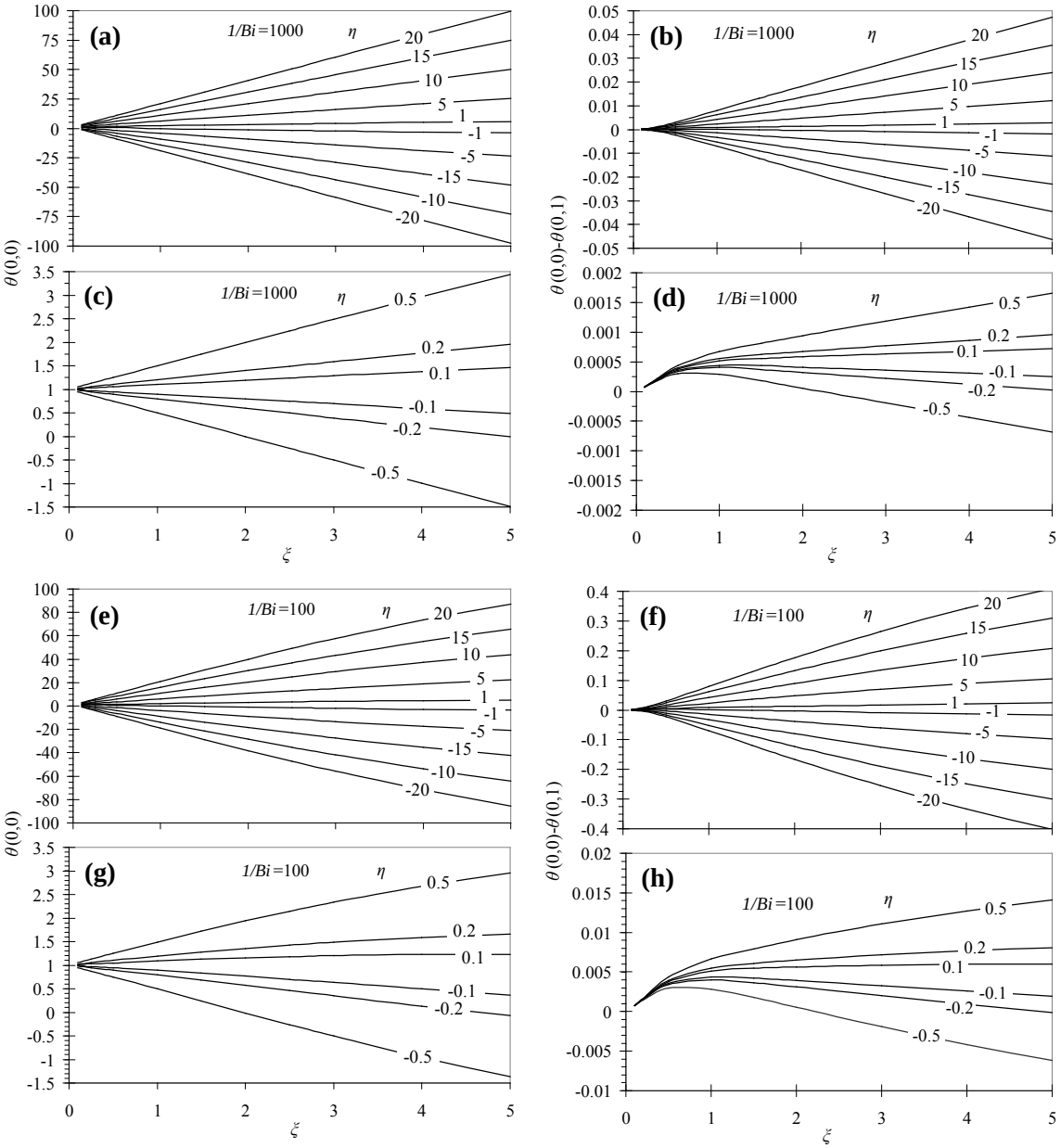

Figure 27. Top surface dimensionless centerline temperature, $\theta(0,0)$, and temperature variation, $\theta(0,0) - \theta(0,1)$, plotted against aspect ratio, ξ, for varying dimensionless heat input, η; (a), (b), (c), (d) $1/Bi$ = 1000 and (e), (f), (g), (h) $1/Bi$ = 100.

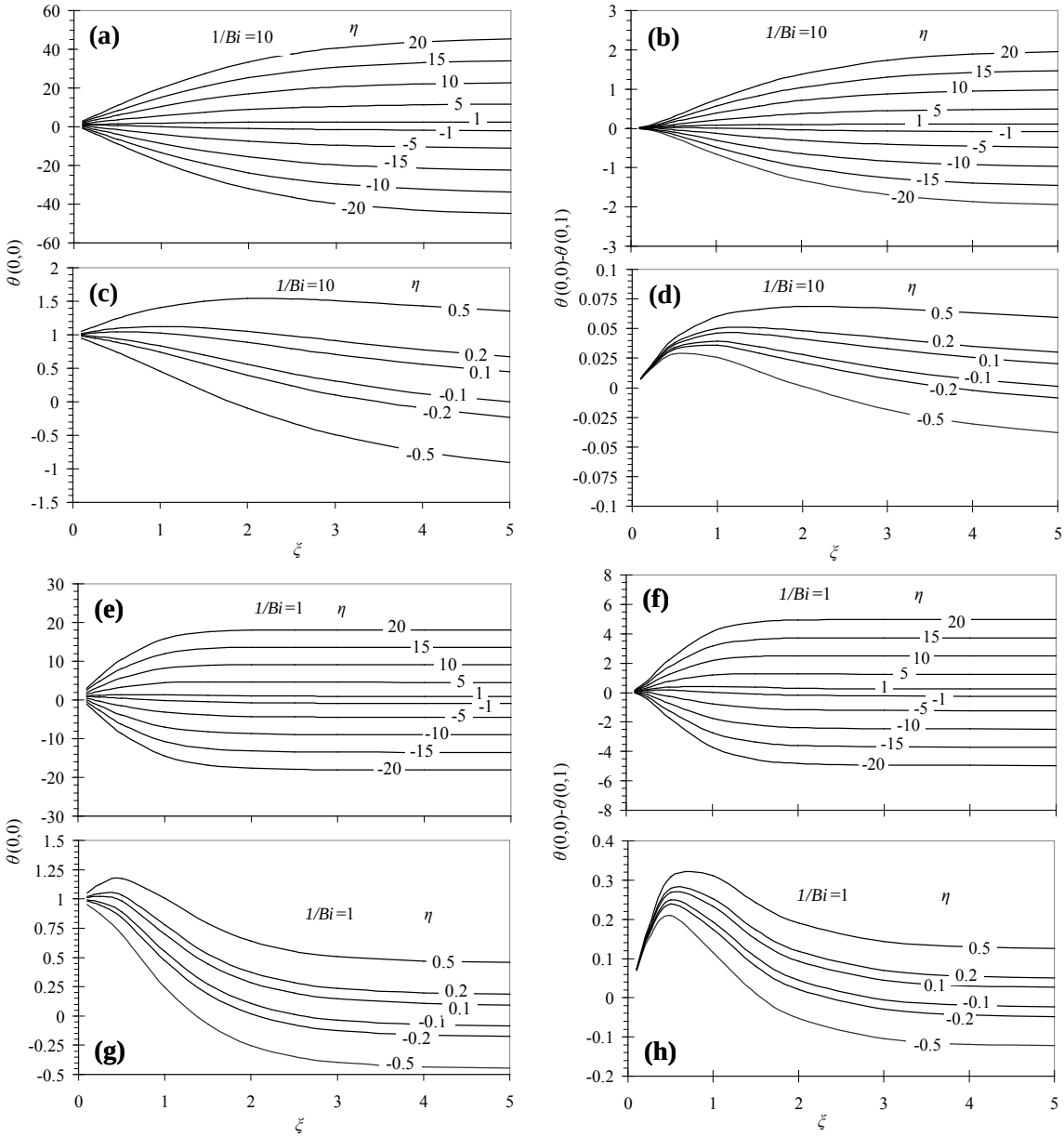

Figure 28. Top surface dimensionless centerline temperature, $\theta(0,0)$, and temperature variation, $\theta(0,0) - \theta(0,1)$, plotted against aspect ratio, ξ, for varying dimensionless heat input, η; (a), (b), (c), (d) $1/Bi = 10$ and (e), (f), (g), (h) $1/Bi = 1$.

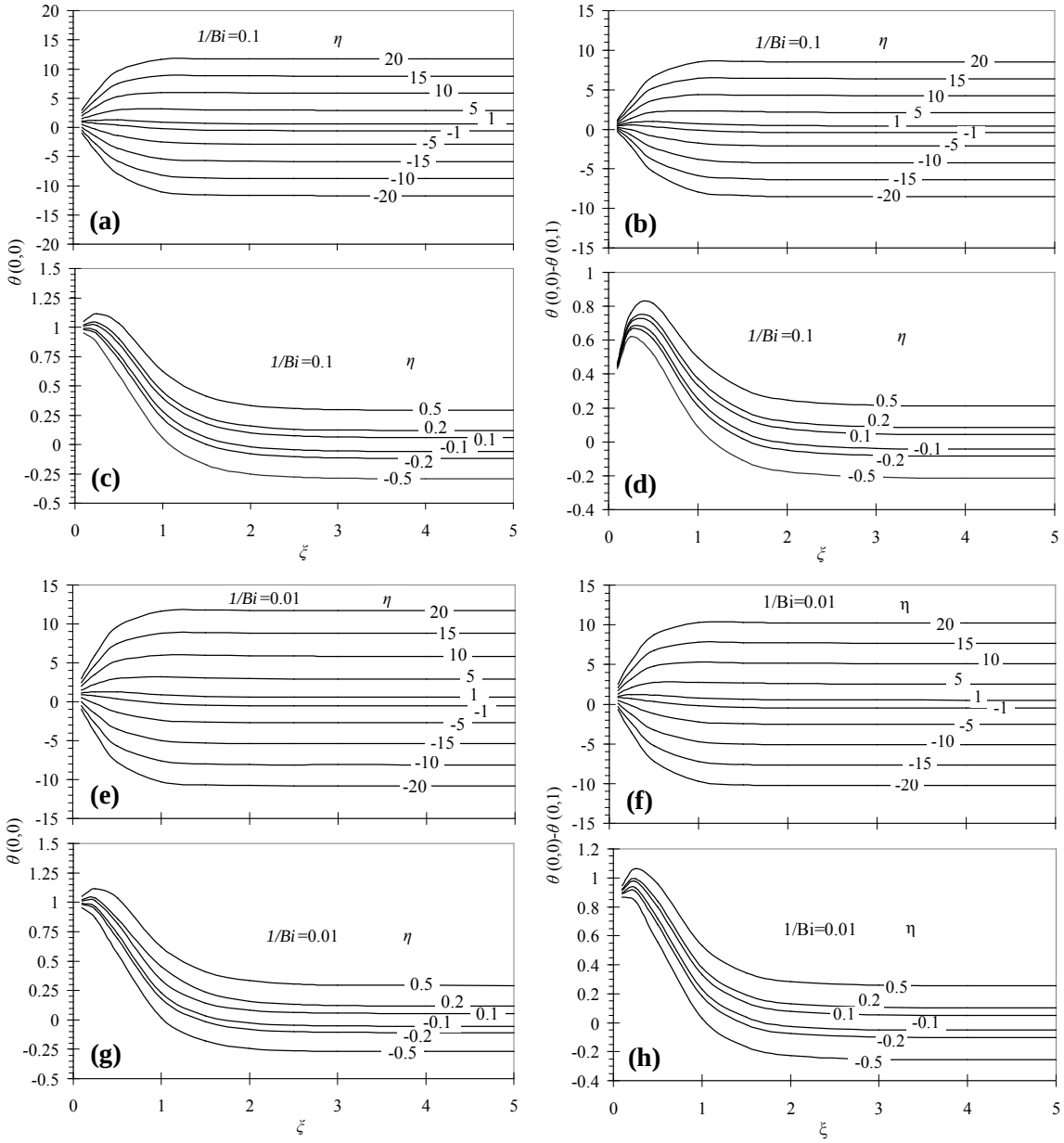

Figure 29. Top surface dimensionless centerline temperature, $\theta(0,0)$, and temperature variation, $\theta(0,0) - \theta(0,1)$, plotted against aspect ratio, ξ, for varying dimensionless heat input, η; (a), (b), (c), (d) $1/Bi = 0.1$ and (e), (f), (g), (h) $1/Bi = 0.01$.

4.3 Comparison of Rectangular and Cylindrical Results

Both rectangular and cylindrical results compare closely with only slight differences. One aspect noted is the fact that there are some unique combinations of dimensionless heat input and aspect ratio combinations that are independent of 1/*Bi*. Figures 30 and 31 show these dimensionless heat input and aspect ratio combinations that are independent of 1/*Bi* for the top surface dimensionless centerline temperature, θ(0,0) and the top surface dimensionless temperature variation, θ(0,0) – θ(0,1). These combinations can be readily determined from Figs. 6-8 and Figs. 20-22, for the rectangular and cylindrical geometries respectively, as the location of the intersection point for the constant 1/*Bi* lines. In the plots shown in Figs. 30 and 31 were generated with constant lines 1/*Bi* = 0.01 and 1000.

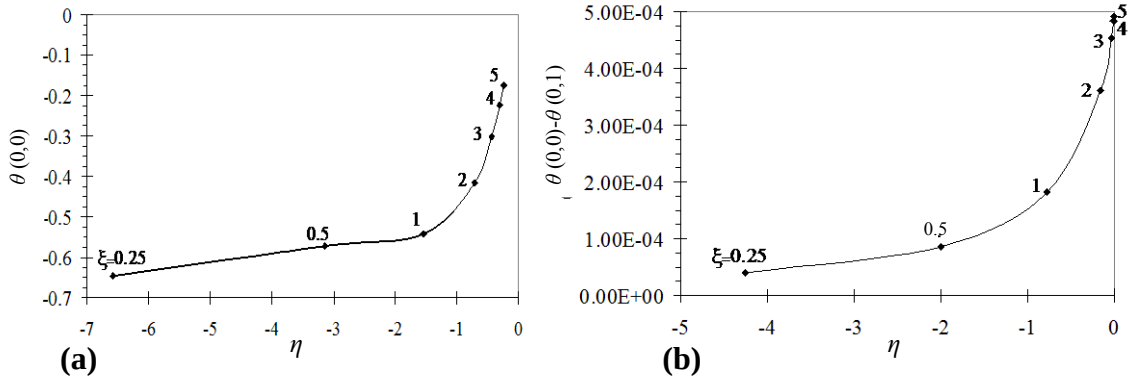

Figure 30. Rectangular dimensionless heat input and aspect ratio combinations that are independent of 1/*Bi* for (a) top surface dimensionless centerline temperature, $\theta(0,0)$ and (b) top surface dimensionless temperature variation, $\theta(0,0) - \theta(0,1)$.

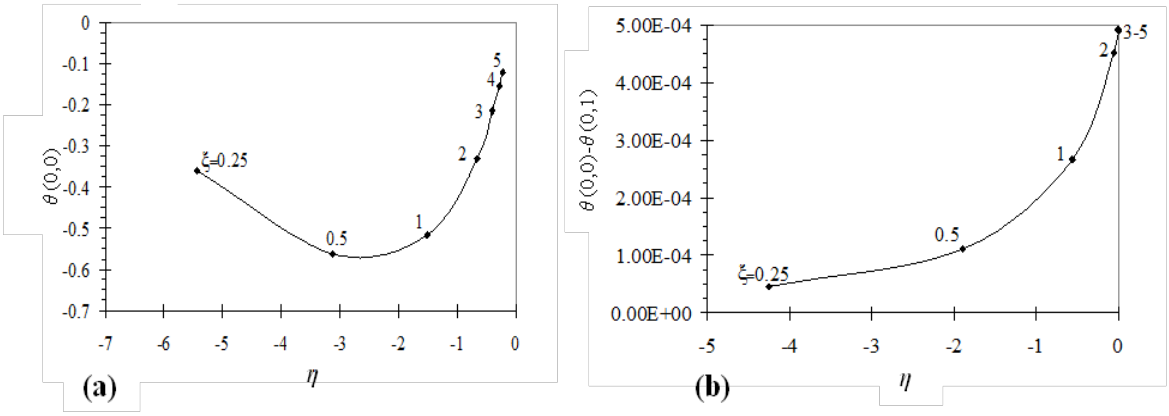

Figure 31. Cylindrical dimensionless heat input and aspect ratio combinations that are independent of 1/*Bi* for (a) top surface dimensionless centerline temperature, $\theta(0,0)$ and (b) top surface dimensionless temperature variation, $\theta(0,0) - \theta(0,1)$.

5.0 CONCLUSION

This analytical study presents results that can be used to determine the effects of boundary condition(s) that will influence the steady-state temperature gradient along the top heated surface of cylindrical and rectangular posts with sidewall cooling. Both dimensional and dimensionless analytical solutions derived and the results are presented in dimensionless graphical form similar to Heisler-Gröber Charts.

This specific example demonstrates how it is possible to determine the cold plate surface and environmental boundary conditions that are required to minimize either the centerline temperature or temperature variation across the heated surface. In this manner, the "best" boundary conditions can be used to specify the cold plate requirements to optimally cool the electronics package. The generated dimensionless plots also allow for easy graphical determination of these boundary conditions as defined in a dimensionless form which can be readily interpreted and used to determine optimal dimensional geometries and/or thermo physical material properties to minimize temperature gradients across a heated electronic surface.

REFERENCES

[1] Yovanovich, M.M., "Thermal Resistances of Circular Source on Finite Circular Cylinder With Side and End Cooling," *Journal of Electronic Packaging*, **125**, 169-177, 2003.

[2] Muzychka, Y.S., Yovanovich, M.M., and Culham, J.R., "Influence of Geometry and Edge Cooling on Thermal Spreading Resistance," *Journal of Thermophysics and Heat Transfer*, **20**, No.2, 247-255, 2006.

[3] Heisler, M.P., "Temperature Charts for Induction and Constant Temperature Heating," *Trans. ASME*, **69**, 227-236, 1947.

[4] Gröber, H., Erk, S., and Grigull, U., *Fundamentals of Heat Transfer*, McGraw-Hill, New York, 1961.

[5] Sha, W.C. and Ganić, E.N., Transient Heat Conduction at Low Biot Numbers: A Supplement to Heisler's Charts," *Letters in Heat and Mass Transfer*, **8**, 379-395, 1981.